Received 25 March 2024; revised 21 April 2024; accepted 23 April 2024. Date of publication 25 April 2024; date of current version 14 May 2024.

*Digital Object Identifier 10.1109/OJCOMS.2024.3393746*

# On the Performance of LoRa Empowered Communication for Wireless Body Area Networks

**MINLING ZHANG [1], GUOFA CAI [1] (Senior Member, IEEE), ZHIPING XU [2] (Member, IEEE), JIGUANG HE [3,4] (Senior Member, IEEE), AND MARKKU JUNTTI [4] (Fellow, IEEE)**

[1]School of Information Engineering, Guangdong University of Technology, Guangzhou 510006, China

[2]School of Ocean Information Engineering, Jimei University, Xiamen 361021, China

[3]Technology Innovation Institute, Abu Dhabi, UAE

[4]The Centre for Wireless Communications, University of Oulu, 90014 Oulu, Finland

CORRESPONDING AUTHOR: G. CAI (e-mail: caiguofa2006@gdut.edu.cn)

This work was supported in part by the National Natural Science Foundation of China under Grant 62071129, and in part by the Academy of Finland through the 6G Flagship Program under Grant 346208.

**ABSTRACT** To remotely monitor the physiological status of the human body, long range (LoRa) communication has been considered as an eminently suitable candidate for wireless body area networks (WBANs). Typically, a Rayleigh-lognormal fading channel is encountered by the LoRa links of the WBAN. In this context, we characterize the performance of the LoRa system in WBAN scenarios with an emphasis on the physical (PHY) layer and medium access control (MAC) layer in the face of Rayleigh-lognormal fading channels and the same spreading factor interference. Specifically, closed-form approximate bit error probability (BEP) expressions are derived for the LoRa system. The results show that increasing the spreading factor (SF) and reducing the interference efficiently mitigate the shadowing effects. Moreover, in the quest for the most suitable MAC protocol for LoRa based WBANs, three MAC protocols are critically appraised, namely the pure ALOHA, slotted ALOHA, and carrier-sense multiple access. The coverage probability, energy efficiency, throughput, and system delay of the three MAC protocols are analyzed in Rayleigh-lognormal fading channel. Furthermore, the performance of the equal-interval-based and equal-area-based schemes is analyzed to guide the choice of the SF. Our simulation results confirm the accuracy of the mathematical analysis, and provide some useful insights for the future design of LoRa based WBANs on how to achieve the desired performance requirements for different conditions (i.e., different network radii and average numbers of end-devices) by using different SF allocation schemes and MAC protocols.

**INDEX TERMS** Wireless body area network, LoRa communication, performance analysis, Rayleigh-lognormal fading channel.

## I. INTRODUCTION

HEALTHCARE Internet of Thing (HIoT) is a highly efficient and convenient way to provide intelligent diagnosis, treat and disease management, and anticipate risks to patient health [1], [2]. Especially, with the rapid spread of COVID-19, HIoT has been adopted to monitor the significant physiological information in the human body [3]. Hence, it is important for HIoT to ensure the low-power, highly reliable, and long-range information transmission.

As an important technology of HIoT, wireless body area network (WBAN) consists of multiple interconnected low-power and resource-constrained sensor devices (e.g., worn, implanted, embedded, swallowed, etc.) that are located in-on-and-around the human body, where these sensor devices are adopted for sensing and data communication [4], [5], [6], [7], [8]. According to [9], in a HIoT system, physiological signals from each sensor device are transmitted to a hub via a WBAN, and then the collected data is forwarded to the service center. Thus, these information can be provided to the

hospitals or clinics. However, due to the limited transmission distance of the WBAN, it is not suitable for long-distance transmission.

Long range (LoRa) modulation, as the physical (PHY) layer of LoRa network, is a chirp spread spectrum (CSS) based modulation, which can achieve low-power and long-range transmission [10], [11]. In the LoRa system, the receiver (usually a gateway) can decode the signal a few decibels below the noise floor. The range and data rate of LoRa communication can be adjusted by different spreading factors (SFs).[1] In addition, LoRa gateway can correctly receive two overlapping signals over the same channel, as long as their SFs are different. Due to these advantages, LoRa modulation was applied in WBAN applications for the off-body communications [12]. In [13] and [14], LoRa sensors were worn on the body to measure the vital signs and environmental data. In [15], a low-power healthcare WBAN platform based on LoRa (HeaLoRa) was proposed for monitoring physiological parameters. In [16], LoRa sensors were placed inside the animal body to monitor the important parameters and communicates with a distant gateway. In such a scenario, the in-to-out-body path loss (PL) was characterized for the first time at 868 MHz. In [17], a low-power LoRa link was built between a fixed base station and a mobile user which is worn on the body. The test results showed that a large range of 1.5 Km can be easily and reliably achieved for off-body LoRa communication links. In [18], the LoRa system was introduced for search and rescue applications in mountain areas. Through the above discussions, it can be found that theoretical analyses of the LoRa system for in-body and off-body communications are still lacking, which limits its further design. In [19], the bit error probability (BEP) expression of the LoRa system was derived over a Rayleigh fading channel. In [20], success probability analysis of the LoRa system was performed over a Rayleigh fading channel. However, for LoRa communication links in the WBAN, a Rayleigh-lognormal fading channel should be applied according to [16], [17], [18].

LoRa wide area network (LoRaWAN) is a medium access control (MAC) protocol designed to run LoRa modulation [21], [22]. According to the LoRaWAN characteristics, the devices generally adopt a pure ALOHA (P-ALOHA) mechanism to access channels [23], where the packets access the channel randomly. In [20], scalability analysis of the LoRa network for P-ALOHA mechanism was performed over Rayleigh fading channels. Although P-ALOHA has simple implementation, it is easy to cause packet collisions. As a consequence, it brings the same SF (defined as *co-SF*) interference, thus significantly affecting the scalability of the LoRa network. To enhance the scalability of LoRa network, the slotted ALOHA (S-ALOHA) and carrier-sense multiple access (CSMA) mechanisms were extensively studied in [24], [25], [26]. In [24], a comparison between P-ALOHA and S-ALOHA protocols in LoRa networks revealed that S-ALOHA enhances network performance in terms of packet loss rate and throughput. In [25], the principle of CSMA for LoRaWAN was presented, where results show that CSMA has lower energy consumption than P-ALOHA, particularly in scenarios involving a large number of devices. Furthermore, in [26], CSMA was found to achieve higher throughput and accommodate larger network capacities compared to P-ALOHA. In [27], the equal-interval-based (EIB) and equal-area-based (EAB) schemes were used to compare and analyze the scalability of LoRa networks. The results show that the scalability of LoRa network is significantly affected by the SF allocation schemes.

Most of the aforementioned studies on PHY and MAC layers of LoRa networks focus on Rayleigh fading channels, and the impact of large-scale fading is ignored [28]. In the LoRa based WBAN, large-scale fading should be taken into account. Motivated by the preliminary investigation in [19], [20], and [28], we propose a more comprehensive and tractable framework of performance analysis on LoRa system for WBAN subject to the Rayleigh-lognormal channels and the *co-SF* interference from the perspective of the PHY and MAC layers. The main contributions of this paper are summarized as follows:

1) A LoRa based WBAN is put forward, which consists of an enormous number of LoRa end-devices (EDs) from the WBANs and a gateway. In such a scenario, the Rayleigh-lognormal channel and the *co-SF* interference are jointly considered.
2) The closed-form BEP expression of the LoRa system for PHY transmission is derived under the Rayleigh-lognormal channel and *co-SF* interference. Furthermore, we investigate the impact of SF, the shadowing standard deviation and the signal-to-interference ratio (SIR) on the BEP. It is shown that although the BEP of the proposed system is significantly affected by the shadowing standard deviation, the system is capable of mitigating the shadowing effects by increasing the SF and SIR.
3) To find the most appropriate MAC protocol for the LoRa based WBAN, the P-ALOHA, S-ALOHA, and NP-CSMA protocols are comprehensively investigated and compared. In addition, to elaborate on the choice of the SFs, the EIB and EAB schemes are considered. Moreover, we analyse the coverage probability, energy efficiency, throughput, and system delay of LoRa networks relying on the above-mentioned protocols and SF allocation schemes for the transmission. Furthermore, we also analyze the impact of some important parameters, i.e., network radius and the average number of EDs, on the system performance.

[1]LoRa adopts multiple chips to encode each information symbol. The SF is defined as the ratio between the chip rate and the information rate, which usually ranges from 7 to 12. For example, when SF is set to 7, there are 128 chips per symbol, whereas SF 12 utilizes up to 4096 chips per symbol.

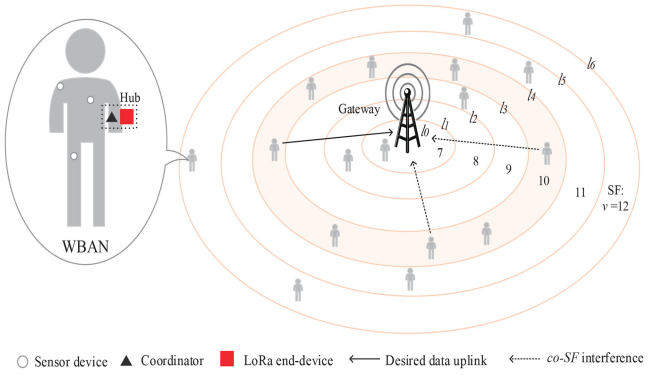


**FIGURE 1.** Uplink transmission for the LoRa based WBAN, where the SF is allocated based on annuli.

The remainder of this paper is organized as follows. Section II introduces the system model of LoRa-based WBAN from the perspective of PHY and MAC layers. In Section III, the performance of the LoRa-based WBAN is analyzed in terms of BEP and some metrics of scalability. Section IV presents the results and discussions. Finally, Section V concludes this paper.

## II. SYSTEM MODEL

Uplink transmission for the LoRa based WBAN is shown in Fig. 1, which includes a large number of LoRa EDs from the WBANs and a gateway. For each WBAN, there are many sensor devices and a hub, where the hub has a coordinator and a LoRa ED. The physiological data collected by the sensor devices is sent to the coordinator. Subsequently, the LoRa EDs send the collected data of the coordinator to the gateway.[2] The EDs are spatially distributed within a circle of radius $R$ (Km), which can be described by *homogeneous Poisson point process* (PPP) $\Phi$ with intensity $\lambda$ ($\lambda$>0) [29]. We assume that $\mathcal{V} \subseteq \mathbb{R}^2$ (2-dimensional (2D) Euclidean space) is the disk of radius $R$, of which the area is $V = |\mathcal{V}| = \pi R^2$. The total number of EDs within the disk is $\mathcal{N}$, which is a random variable following a Poisson distribution with mean $\overline{\mathcal{N}} = \lambda V$. The probability density function (PDF) of the distance between the randomly selected ED and the gateway can be expressed as $f_{\mathrm{ED}}(x) = \frac{2\pi x}{\pi R^2}$, $0 \le x \le R$. The disk is divided into $K$ parts, each of which corresponds to a different SF $\nu$, where $\nu \in \Psi = \{7, 8, 9, 10, 11, 12\}$ and $K = |\Psi|$ represents the number of annuli with $|\cdot|$ being the cardinality of a set. It should be noted that the signals from different annuli are perfectly orthogonal, and we only consider the interfering EDs assigned with the same SF. The inner and outer diameters of the $j$-th ($1 \le j \le K$) annulus are defined as $l_{j-1}$ and $l_j$, respectively.

In practical scenarios, wireless 3D network models can be considered, whose spatial location is modeled as a 3D PPP with intensity $\lambda$ [30]. In such a network, it is assumed that the gateway is located at the origin of the 3D Cartesian coordinate system, and the EDs are spatially distributed within a sphere of radius $R$. Without loss of generality, let $\mathbf{w}_i = [r_i, \vartheta_i, \varphi_i]^T$, $i = 1, \ldots, \overline{\mathcal{N}}$ denote the 3D location of the ED in spherical coordinates, and $\mathbf{w}_i^c = [r_i \cos(\varphi_i) \sin(\vartheta_i), r_i \sin(\varphi_i) \sin(\vartheta_i), r_i \cos(\vartheta_i)]^T$ denote that in Cartesian coordinates. Hence, the Euclidean distance between the ED and the gateway can be calculated as $\|\mathbf{w}_i^c\|$, where $\|\cdot\|$ represents the Euclidean norm. The PDF of the distance between the randomly selected ED and the gateway is given by [31], i.e., $f_{ED}(x) = 3x^2 \frac{(R^3 - x^3)}{R^3}$, $0 \le x \le R$. Then, the SFs are assigned to EDs based on the distance between the EDs and the gateway.

To facilitate the subsequent analysis, a 2D network model is adopted in this paper. We leave the task of analysising the performance of 3D network as our future work.

### A. SIGNAL MODEL FOR LORA PHYSICAL LAYER

LoRa modulation is based on CSS. If the bandwidth of chirp signal is $B$, a LoRa sample is sent every elapsed time $T = \frac{1}{B}$. Besides, LoRa modulation is realized by spreading the frequency change of the chirp signal over $2^\nu$ samples within a symbol duration $T_s = 2^\nu T$. Each symbol $s_q$ can carry $\nu$ bits of information and $s_q = q$, $q \in \{0, 1, 2, \ldots, 2^\nu - 1\}$. The chirp signal $\varpi_q(mT)$ can be expressed as

$$\varpi_q(mT) = \sqrt{\frac{1}{2^\nu}} e^{j2\pi[(q+m) \bmod 2^\nu]\frac{m}{2^\nu}}, \tag{1}$$

where $m = 0, 1, 2, \cdots, 2^\nu - 1$ indicates the symbol index at time $mT$. Moreover, the transmitted discrete-time LoRa baseband signal can be expressed as [19]

$$\begin{aligned} \omega_q(mT) &= \sqrt{E_s}\varpi_q(mT) \\ &= \sqrt{\frac{E_s}{2^\nu}} e^{j2\pi[(q+m) \bmod 2^\nu]\frac{m}{2^\nu}}, \end{aligned} \tag{2}$$

where $E_s$ is the energy per symbol.

From [19], based on the orthogonality of chirp signals with different offsets, the cross-correlation property of the LoRa demodulator is written as

$$C_{\iota,q} = \sum_{m=0}^{2^\nu - 1} \varpi_q(mT)\varpi_\iota^*(mT) = \begin{cases} 1, & \iota = q \\ 0, & \iota \ne q \end{cases}, \tag{3}$$

where the chirp signal $\varpi_\iota(mT)$ is used to transmit a symbol $s_\iota = \iota$, $\iota \in \{0, 1, 2, \ldots, 2^\nu - 1\}$, and $\varpi_\iota^*(mT)$ is the complex conjugate of the chirp signal $\varpi_\iota(mT)$.

Due to the human body shadows and environmental hindrances, the communication channel can be modeled as a Rayleigh-lognormal fading channel [32]. Since the LoRa transmitters generally work asynchronously, collisions always occur between different signals. At the gateway, the received signal can be represented as

$$r_q(mT) = h_1\omega_q(mT) + \sum_{k=2}^{\mathcal{N}} \chi_k^\nu h_k \omega_{I,k}(mT) + \phi_q(mT), \tag{4}$$

[2]Human movement can cause blockages, thus weak LoRa packets may not be correctly detected. We leave the task of improving LoRa reception performance as our future work.

where $h_1$ and $h_k$ represent the channel coefficient between the desired ED and the gateway, and that between the interfering ED and the gateway, respectively. $\chi_k^{\nu}$ is the output of the indicator function, where $\chi_k^{\nu} = 1$ if the $k$-th interfering node within the same SF annulus as the desired ED, otherwise $\chi_k^{\nu} = 0$. $\omega_q(mT)$ is the desired signal, $\omega_{I,k}(mT)$ is the interfering signal from the $k$-th interfering node, and $\phi_q(mT)$ is complex additive white Gaussian noise (AWGN) with zero-mean and variance $N_0$.

Since the strongest interfering signal typically dominates the impact when multiple interfering signals collide at the same time [33], we only need to consider the strongest interfering signal in this paper. According to [27], there is only a small decline in the performance when considering all co-SF interfering signals, compared with considering only the strongest interfering signal. To simplify the analysis, we assume that there exists only one strongest interfering signal. Let $h_{\hat{k}}$ denote the channel coefficient between the strongest interfering ED and the gateway, and $\omega_{I,\hat{k}}(mT)$ denotes the strongest interfering signal, (4) can be expressed as

$$r_q(mT) = h_1\omega_q(mT) + h_{\hat{k}}\omega_{I,\hat{k}}(mT) + \phi_q(mT). \tag{5}$$

The log-distance PL model between an ED and a gateway is given by

$$P_L(d) = P_L(d_0) + 10n\log_{10}\frac{d}{d_0} + S[dB], \tag{6}$$

where $P_L(d_0)$ is the PL in dB at the reference distance $d_0 = 1$ m, $d$ is the distance between the ED and the gateway, $n$ is the PL exponent and $S \sim \mathcal{N}(0, \sigma_{dB}^2)$ is a normally distributed random variable that represents the shadowing effect.

Without loss of generality, combining the fading with the shadowing, the instantaneous normalized channel power $|h|^2$ can be given by

$$\begin{aligned} |h|^2 &= |h_{\text{ray}}|^2 |h_{\log}|^2 \\ &= |h_{\text{ray}}|^2 10^{-\frac{P_L(d)[dB]}{10}} \\ &= |h_{\text{ray}}|^2 10^{-\frac{P_L(d_0)+10n\log_{10}\frac{d}{d_0}}{10}} \times 10^{-\frac{S}{10}} \\ &= |h_{\text{ray}}|^2 Hg(d) \\ &= |\hbar|^2 g(d), \end{aligned} \tag{7}$$

where $|h_{\text{ray}}|^2$ is the channel power gain of a Rayleigh channel modelling as an exponential random variable with mean one, i.e., $|h_{\text{ray}}|^2 \sim \exp(1)$. $|h_{\log}|^2$ represents the channel power gain of a log-normal channel. $H = 10^{-\frac{S}{10}}$ follows a log-normal distribution with mean $\mu_H = 0$ and standard deviation $\sigma_H = \frac{\ln 10}{10}\sigma_{dB}$. $g(d) = 10^{-\frac{P_L(d_0)+10n\log_{10}\frac{d}{d_0}}{10}}$ is the path loss attenuation, and $|\hbar|^2 = |h_{\text{ray}}|^2 H$ follows a Rayleigh-lognormal distribution. Hence, (5) can be further written as

$$\begin{aligned} r_q(mT) = &\sqrt{|\hbar_1|^2 g(d_1)}\omega_q(mT) \\ &+ \sqrt{|\hbar_{\hat{k}}|^2 g(d_{\hat{k}})}\omega_{I,\hat{k}}(mT) + \phi_q(mT), \end{aligned} \tag{8}$$

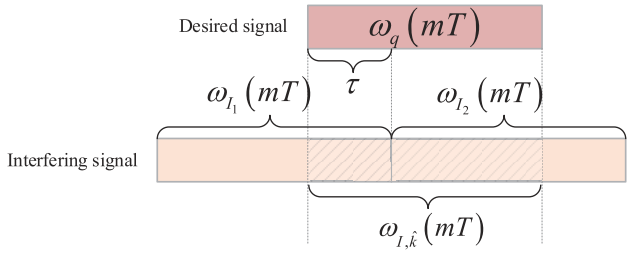


**FIGURE 2.** Illustration of the relationship between the desired signal and the interfering signal.

where $\hbar_1$ and $\hbar_{\hat{k}}$ represent the channel gain of Rayleigh-lognormal channel between the desired ED and the gateway, and that between the strongest interfering ED and the gateway, respectively. $d_1$ and $d_{\hat{k}}$ denote the distance between the desired ED and the gateway, and that between the strongest interfering ED and the gateway, respectively.

Besides, the correlator output of the LoRa demodulator is given by

$$\begin{aligned} \mathrm{O}_\iota &= \sum_{m=0}^{2^\nu-1} r_q(mT)\varpi_\iota^*(mT) \\ &= \begin{cases} \sqrt{\beta_1 E_s g(d_1)} + \sqrt{\beta_{\hat{k}} E_s g(d_{\hat{k}})}\Delta_\iota + \phi_\iota(mT), & \iota = q \\ \sqrt{\beta_{\hat{k}} E_s g(d_{\hat{k}})}\Delta_\iota + \phi_\iota(mT), & \iota \neq q \end{cases}, \end{aligned} \tag{9}$$

where $\beta_1 = |\hbar_1|^2$, $\beta_{\hat{k}} = |\hbar_{\hat{k}}|^2$, $\phi_\iota(mT)$ is also complex AWGN with zero-mean and variance $N_0$, and $\Delta_\iota$ is the cross-correlation interference.

Fig. 2 shows the relationship between the desired signal and the interfering signal. According to [34] and this figure, the interfering signal is defined as

$$\omega_{I,\hat{k}}(mT) = \begin{cases} \frac{1}{\sqrt{\rho}}\omega_{I_1}(mT), & 0 \le m < \tau \\ \frac{1}{\sqrt{\rho}}\omega_{I_2}(mT), & \tau \le m < 2^\nu \end{cases}, \tag{10}$$

where $\omega_{I,\hat{k}}(mT)$ consists of two signals $\omega_{I_1}(mT)$ and $\omega_{I_2}(mT)$, $I_1, I_2 \in \{0, 1, 2, \ldots, 2^\nu - 1\}$, $\rho$ represents the SIR, and it is assumed that a random offset $\tau$ occurs between the desired and interfering signal $\omega_{I_2}(mT)$. Without loss of generality, $\tau$ is assumed to be uniformly distributed in $[0, 2^{\nu-1}]$, thus, it can ensure that the number of interfering samples from $\omega_{I_2}(mT)$ is larger than that from $\omega_{I_1}(mT)$.

Accordingly, one can assume $I_2 = 0$ to ensure that the last $2^\nu - \tau$ samples of $\omega_q(mT)$ are interfered by the signal $\omega_0(mT) = \sqrt{\frac{E_s}{2^\nu}} e^{j2\pi(m)\frac{m}{2^\nu}}$ according to (2). Hence, $\Delta_\iota$ can be expressed as

$$\Delta_\iota = \frac{1}{\sqrt{\rho}}\left( C_{\iota,I_1}\big|_0^{\tau-1} + C_{\iota,0}\big|_\tau^{2^\nu-1} \right), \tag{11}$$

where

$$C_{\iota,I_1}\big|_0^{\tau-1} = \frac{1}{2^\nu}\sum_{m=0}^{\tau-1} e^{j2\pi(\iota-I_1)\frac{m}{2^\nu}}, \tag{12}$$

$$C_{\iota,0}\big|_{\tau}^{2^{\nu}-1} = \frac{1}{2^{\nu}} \sum_{m=\tau}^{2^{\nu}-1} e^{j2\pi\iota\frac{m}{2^{\nu}}}. \tag{13}$$

Using the summation formula of the geometric sequence, the Euler's formula and the trigonometric formula, the magnitude of $C_{\iota,I_1}|_0^{\tau-1}$ and $C_{\iota,0}|_{\tau}^{2^{\nu}-1}$ can be expanded as

$$\left| C_{\iota,I_1}\big|_0^{\tau-1} \right| = \frac{1}{2^{\nu}} \left| \frac{\sin\left(\pi \frac{(\iota-I_1)}{2^{\nu}}\tau\right)}{\sin\left(\pi \frac{(\iota-I_1)}{2^{\nu}}\right)} \right|, \tag{14}$$

$$\left| C_{\iota,0}\big|_{\tau}^{2^{\nu}-1} \right| = \frac{1}{2^{\nu}} \left| \frac{\sin\left(\pi \frac{\iota}{2^{\nu}}(2^{\nu}-\tau)\right)}{\sin\left(\pi \frac{\iota}{2^{\nu}}\right)} \right|, \tag{15}$$

where $|C_{\iota,I_1}|_0^{\tau-1}|$ reaches its maximum value of $\frac{\tau}{2^{\nu}}$ when $\iota = I_1$, and $|C_{\iota,0}|_{\tau}^{2^{\nu}-1}|$ reaches its maximum value of $\frac{2^{\nu}-\tau}{2^{\nu}}$ when $\iota = 0$.

Let $\mathcal{U}_{\iota}$ be the upper bound of the magnitude of $\Delta_{\iota}$. It can be given by

$$|\Delta_{\iota}| \le \mathcal{U}_{\iota} = \frac{1}{2^{\nu}\sqrt{\rho}} \left( \left| \frac{\sin\left(\pi \frac{(\iota-I_1)}{2^{\nu}}\tau\right)}{\sin\left(\pi \frac{(\iota-I_1)}{2^{\nu}}\right)} \right| + \left| \frac{\sin\left(\pi \frac{\iota}{2^{\nu}}(2^{\nu}-\tau)\right)}{\sin\left(\pi \frac{\iota}{2^{\nu}}\right)} \right| \right). \tag{16}$$

For each realization of $I_1$ and $\tau$, one can assume that $\mathcal{U}_{\iota}$ achieves the peak cross-correlation interference at some bin $\tilde{\iota} = \arg\max_{\iota}(\mathcal{U}_{\iota})$. The cross-correlation interference terms are negligible when $\iota \neq \tilde{\iota}$. Hence, $\mathcal{U}_{\iota}$ can be approximated as

$$\mathcal{U}_{\iota} \approx \begin{cases} \mathcal{U}_{\tilde{\iota}}, & \iota = \tilde{\iota} \\ 0, & \iota \neq \tilde{\iota} \end{cases}. \tag{17}$$

Accordingly, since $\tau \in [0, 2^{\nu-1}]$, the peak cross-correlation interference is most likely to occur at bin $\tilde{\iota} = 0$, and one has

$$\mathcal{U}_{\tilde{\iota}} \approx \mathcal{U}_0 = \frac{1}{2^{\nu}\sqrt{\rho}} \left( \left| \frac{\sin\left(\pi \frac{(\iota-I_1)}{2^{\nu}}\tau\right)}{\sin\left(\pi \frac{(\iota-I_1)}{2^{\nu}}\right)} \right| + \left(2^{\nu}-\tau\right) \right). \tag{18}$$

Finally, combining (9), (17) and (18), the magnitude of the correlator output of the LoRa demodulator can be obtained as

$$\left|\mathrm{O}_{\iota}|q=0\right| \approx \begin{cases} \left| \sqrt{\beta_1 E_s g(d_1)} + \sqrt{\beta_{\hat{k}} E_s g(d_{\hat{k}})}\mathcal{U}_0 + \phi_0(mT) \right|, & \iota = 0 \\ |\phi_{\iota}(mT)|, & \iota \neq 0 \end{cases}, \tag{19}$$

$$\left|\mathrm{O}_{\iota}|q\neq 0\right| \approx \begin{cases} \left| \sqrt{\beta_{\hat{k}} E_s g(d_{\hat{k}})}\mathcal{U}_0 + \phi_0(mT) \right|, & \iota = 0 \\ \left| \sqrt{\beta_1 E_s g(d_1)} + \phi_q(mT) \right|, & \iota = q \\ |\phi_{\iota}(mT)|, & \iota \neq 0, q \end{cases}. \tag{20}$$

We select the index of the correlator output which attains the largest amplitude. Therefore, the detected symbol $\tilde{s}_q$ is written as

$$\tilde{s}_q = \arg\max_{\iota}(|\mathrm{O}_{\iota}|). \tag{21}$$

**TABLE 1.** The parameters for SF allocation schemes.

| Parameters | EIB | EAB |
|---|---|---|
| Width | $r_j = \frac{R}{K}$ | $r_j = R\sqrt{\frac{j}{K}} - R\sqrt{\frac{j-1}{K}}$ |
| Area | $\lvert\mathcal{V}_j\rvert = \pi\left(\frac{R}{K}\right)^2(2j-1)$ | $\lvert\mathcal{V}_j\rvert = \frac{\pi R^2}{K}$ |

### B. LORA MAC LAYER

In the distance-based SF allocation scheme, a value of the SF is assigned for an ED based on the distance between the ED and the gateway. Firstly, the LoRa network is divided into $K$ co-center annuli centering on the gateway. Secondly, the SFs are assigned to the annuli from the gateway to the outermost boundary of the LoRa network in an ascending order from low to high. Two types of distance-based SF allocation schemes, i.e., EIB and EAB, are considered in this paper. The EIB scheme has equal-width of each annulus while the EAB scheme has equal-area of each annulus. The parameters of the two schemes are shown in Table 1.

The traditional channel access mechanism for LoRa is P-ALOHA, which is easy to implement. However, due to its poor scalability, alternative access mechanisms can be considered. The purpose of this paper is to investigate the performance of different access mechanisms, i.e., P-ALOHA, S-ALOHA and NP-CSMA. According to [28], we can define the intensity $\lambda_u$ of the PPP of interferers $\Phi_u$ for $u \in \{\text{P-ALOHA, S-ALOHA, NP-CSMA}\}$.

#### 1) P-ALOHA

For P-ALOHA, when a user intends to send a message, the message is fed into the channel immediately. Due to the broadcast nature of the channel, the transmission is successful if no collision occurs. Conversely, the transmission fails and a retransmission is required. For P-ALOHA, one can express the intensity of the interferers as

$$\lambda_{\text{P-ALOHA}} = 2\alpha\lambda, \tag{22}$$

where '2' means the vulnerability time of P-ALOHA is twice of the message time-on-air (ToA) and $\alpha$ is the duty cycle constraint.

#### 2) S-ALOHA

In the S-ALOHA protocol, time is segmented into uniform time slots, with all users accessing the channel simultaneously at the beginning of each slot. In the event of a collision, transmission is deferred until the beginning of the subsequent time slot. The collision is divided into intra-slot collision and inter-slot collision, where the inter-slot collision is divided into the collision with the previous time slot and that with the next time slot. Hence, one can obtain the intensity of the interferers as

$$\lambda_{\text{S-ALOHA}} = \left(1 + \frac{T_g}{T_o}\right) p_s \alpha\lambda, \tag{23}$$

where $T_g$ is the guard interval, $T_o$ is the value of ToA, $p_s = 1 + Q(\frac{T_g+T_p-5T_s}{\sqrt{2}\sigma_{te}}) + Q(\frac{T_g}{\sqrt{2}\sigma_{te}})$ is the total probability

of collisions, $Q(x) = \frac{1}{\sqrt{2\pi}} \int_x^\infty e^{-\frac{\varsigma^2}{2}} d\varsigma$ is the $Q$-function, $T_p$ is the message preamble duration, and $\sigma_{te}$ is the standard deviation of packet lengths.

Since we consider low data rate optimization mode, $T_o$ is given in (24), as shown at the bottom of the page, where $N_{bp}$ is the payload size for the message, $N_{sp}$ is the length of the message preamble, $N_{CRC} = 16$ if cyclic redundancy check (CRC) is activated, otherwise $N_{CRC} = 0$. $N_{sh} = 20$ is for explicit header, $N_{sh} = 0$ is for implicit header, and $cr = 1$, 2, 3 or 4 is associated with coding rate $CR = 4/5$, 4/6, 4/7 or 4/8.

#### 3) NP-CSMA

In NP-CSMA, the channel is assessed prior to transmission. If the channel is clear, data is promptly transmitted. Conversely, if the channel is busy, it must wait for an arbitrary duration before sending the frame when the channel becomes available. According to [28], one has

$$\lambda_{\text{NP-CSMA}} = \left(2 - \frac{T_p - 5T_s}{T_o}\right)(1 - \Xi)\frac{1 - e^{-E(n_A)}}{E(n_A)} p\lambda, \quad (25)$$

where $\frac{T_p - 5T_s}{T_o}$ is the reduction of vulnerability time due to the nature of LoRa transmission, $p$ is the probability for an ED to be granted access to the channel ($p > \alpha$), $E(n_A)$ is the expected number of neighbours of an interfering ED, $\Xi$ is the proportion of EDs in the annulus within the contention of transmiter, expressed as $\Xi = \int_0^{2l_j} [1 - F(\frac{\mathcal{P}_0}{\mathcal{P}_{\text{tx}} g(x)})] f_{\mathfrak{R}}(x) dx$, where $F(\cdot)$ is the cumulative distribution function (CDF) of Rayleigh-lognormal distribution, $\mathcal{P}_0$ is the detection threshold, $\mathcal{P}_{\text{tx}}$ is the power consumption of an ED when transmitting the data and $f_{\mathfrak{R}}(x)$ is the distance distribution of two independent random EDs uniformly distributed inside a circle of radius $\mathfrak{R}$ [35], i.e., $f_{\mathfrak{R}}(x) = \frac{4x}{\pi \mathfrak{R}^2}[\cos^{-1}(\frac{x}{2\mathfrak{R}}) - \frac{x}{2\mathfrak{R}}\sqrt{1 - \frac{x^2}{4\mathfrak{R}^2}}]$, $0 \le x \le 2\mathfrak{R}$.

## III. PERFORMANCE ANALYSES

In this section, we comprehensively evaluate the performance of LoRa based WBANs in terms of BEP, success probability, coverage probability, energy efficiency, throughput, and system delay.

### A. BEP ANALYSIS

The received signal-to-noise ratio (SNR) is given by

$$\gamma = \frac{E_s/T_s}{BN_0}|h|^2 = \frac{E_s g(d)}{N_0 2^\nu}|\hbar|^2 = \frac{\mathcal{P}_{\text{tx}} g(d)}{N}|\hbar|^2, \quad (26)$$

where $N = -174 + \eth + 10\log_{10} B$ dBm, $\eth$ is the noise figure of receiving equipment and is fixed for a particular hardware implementation as 6 dB, and $\overline{\gamma} = \frac{E_s g(d)}{N_0 2^\nu}$ is the average SNR.

The PDFs of power gains for the Rayleigh fading channel and shadowing are respectively written as

$$p_{\text{ray}}(x) = e^{-x}, \quad (27)$$

$$p_{\log}(x) = \frac{1}{\sqrt{2\pi}\sigma_H x} e^{-\frac{(\ln x - \mu_H)^2}{2\sigma_H^2}}. \quad (28)$$

Using a gamma distribution to approximate the log-normal distribution [36], one can obtain

$$p_{\log}(x) \approx \frac{1}{\Gamma(\psi)}\left(\frac{\psi}{\varepsilon}\right)^\psi x^{\psi-1} e^{-x\frac{\psi}{\varepsilon}}, \quad (29)$$

where $\Gamma(\cdot)$ is the gamma function, $\psi = \frac{1}{e^{\sigma_H^2} - 1}$ and $\varepsilon = e^{\mu_H}\sqrt{\frac{\psi+1}{\psi}}$.

Let $\beta = |\hbar|^2 = |h_{\text{ray}}|^2 H$, according to [37] and [38], the PDF of $\beta$ can be computed as

$$p_\beta(z) \approx p_{\text{ray}}(z) \times p_{\log}(z) = \frac{z^{\xi-1}}{\Gamma(\xi)\delta^\xi} e^{-\frac{z}{\delta}}, \quad (30)$$

where $\xi = \frac{1}{2e^{\sigma_H^2} - 1}$ and $\delta = (2e^{\sigma_H^2} - 1)e^{\mu_H}\sqrt{e^{\sigma_H^2}}$.

Using $\int_0^z x^t e^{-\varsigma x} dx = \varsigma^{-t-1}\mathcal{G}(t+1, \varsigma z)$, the approximated CDF of $\beta$ can be calculated as

$$F_\beta(z) = \int_{-\infty}^z p_\beta(x) dx \approx \frac{1}{\Gamma(\xi)}\mathcal{G}\left(\xi, \frac{z}{\delta}\right), \quad (31)$$

where $\mathcal{G}(\cdot,\cdot)$ is the lower incomplete gamma function.

According to the analysis in Section II-A, the BEP of the LoRa system over a Rayleigh-lognormal fading channel with *co-SF* interference can be given by

$$\begin{aligned} P_b &= \frac{2^{\nu-1}}{2^\nu - 1} P_e \\ &\overset{(a)}{\approx} \frac{1}{2}\left(\frac{1}{2^\nu} P_e|\iota = 0 + \frac{2^\nu - 1}{2^\nu} P_e|\iota \neq 0\right) \\ &\overset{(b)}{\approx} \frac{1}{2}\left(\frac{2^\nu - 1}{2^\nu} P_e|\iota \neq 0\right) \\ &\overset{(c)}{\approx} \frac{1}{2}\left(1 - \left(1 - P_e^{(\text{N})}\right)\left(1 - P_e^{(\text{I})}\right)\right) \\ &\approx \frac{1}{2}\left(P_e^{(\text{N})} + \left(1 - P_e^{(\text{N})}\right)P_e^{(\text{I})}\right), \end{aligned} \quad (32)$$

where $P_e$ represents the corresponding symbol error probability (SEP), $P_e^{(\text{N})}$ and $P_e^{(\text{I})}$ denote the SEP over a Rayleigh-lognormal fading channel in the case of no interference and *co-SF* interference, respectively. Here, in step (a), $\frac{2^{\nu-1}}{2^\nu - 1}$ approximates to $\frac{1}{2}$, and $P_e$ is evaluated in terms of the conditional probabilities $P_e|\iota = 0$. and $P_e|\iota \neq 0$. In step (b), the BEP is assumed to be determined by the case of $\iota \neq 0$, i.e., the magnitude of the correlator output can

$$T_o = T_s \times \left[N_{sp} + 4.25 + 8 + \left\lceil\left(\frac{\max(8N_{bp} + N_{CRC} - 4\nu + 8 + N_{sh}, 0)}{4(\nu - 2)}\right)\right\rceil \times (cr + 4)\right], \quad (24)$$

be approximated as (20). In step (c), $\frac{2^{\nu}-1}{2^{\nu}}$ is approximated to be 1, and $.P_e|\iota \neq 0$ is expressed by $P_e^{(\mathrm{N})}$ and $P_e^{(\mathrm{I})}$.

Firstly, according to [19], $P_e^{(\mathrm{N})}$ can be given by

$$\begin{aligned} P_e^{(\mathrm{N})} &= \int_0^{\infty} Q\left(\sqrt{2^{\nu+1}\overline{\gamma}x} - \sqrt{2H_{2^{\nu}-1}}\right) p_{\beta}(x)dx \\ &\approx \int_0^{\infty} Q\left(\sqrt{2^{\nu+1}\overline{\gamma}x} - \sqrt{2H_{2^{\nu}-1}}\right) \frac{x^{\xi-1}}{\Gamma(\xi)\delta^{\xi}} e^{-\frac{x}{\delta}} dx, \end{aligned} \tag{33}$$

where $H_{\varsigma} \approx \ln(\varsigma) + \frac{1}{2\varsigma} + 0.57722$.

Using the linear approximation and some mathematical calculations [39], $Q(\sqrt{2^{\nu+1}\overline{\gamma}x} - \sqrt{2H_{2^{\nu}-1}})$ in (33) can be approximated as

$$\begin{aligned} &Q\left(\sqrt{2^{\nu+1}\overline{\gamma}x} - \sqrt{2H_{2^{\nu}-1}}\right) \\ &\approx \begin{cases} 1, & x \leq a + \frac{1}{2b} \\ \frac{1}{2} + b(x-a), & a + \frac{1}{2b} < x < a - \frac{1}{2b} \\ 0, & x \geq a - \frac{1}{2b} \end{cases}, \end{aligned} \tag{34}$$

where $a = \frac{H_{2^{\nu}-1}}{2^{\nu}\overline{\gamma}}$ and $b = -\frac{2^{\nu}\overline{\gamma}}{2\sqrt{\pi H_{2^{\nu}-1}}}$.

Then, (33) can be written as

$$\begin{aligned} P_e^{(\mathrm{N})} \approx &\int_0^{a+\frac{1}{2b}} \frac{x^{\xi-1}}{\Gamma(\xi)\delta^{\xi}} e^{-\frac{x}{\delta}} dx \\ &+ \int_{a+\frac{1}{2b}}^{a-\frac{1}{2b}} \left(\frac{1}{2} + b(x-a)\right) \frac{x^{\xi-1}}{\Gamma(\xi)\delta^{\xi}} e^{-\frac{x}{\delta}} dx. \end{aligned} \tag{35}$$

By merging the same parts of the integration interval, the closed-form approximation of $P_e^{(\mathrm{N})}$ can be given in (36), as shown at the bottom of the page.

Secondly, according to the deduced formula of the SEP over AWGN channel in [40], $P_e^{(\mathrm{I})}$ can be calculated as (37), as shown at the bottom of the page. The double integral part in (37) is denoted by $P_e^{(\mathrm{I})}|_{\mathcal{U}_0}$..

Since double integral is very complicated, we firstly integrate it with respect to $\beta_1$. Let $A = \sqrt{2^{\nu}\overline{\gamma}\beta_{\hat{k}}}\mathcal{U}_0$, and according to the Hermite integration in [41, Table 25.10], one can obtain

$$\begin{aligned} &\int_0^{\infty} Q\left(\sqrt{2^{\nu}\overline{\gamma}\beta_1} - A\right) p_{\beta}(\beta_1)d\beta_1 \\ &\approx \int_0^{\infty} Q\left(\sqrt{2^{\nu}\overline{\gamma}\beta_1} - A\right) \frac{{\beta_1}^{\xi-1}}{\Gamma(\xi)\delta^{\xi}} e^{-\frac{\beta_1}{\delta}} d\beta_1 \\ &\approx \int_{-\infty}^{+\infty} Q\left(\sqrt{2^{\nu}\overline{\gamma}e^{y_1}} - A\right) \frac{e^{y_1(\xi-1)}}{\Gamma(\xi)\delta^{\xi}} e^{-\frac{e^{y_1}}{\delta}} e^{y_1} dy_1 \\ &\approx \sum_{w_1=1}^{W_1} \zeta_{w_1} e^{{y_1}^2} e^{y_1\xi - \frac{e^{y_1}}{\delta}} \frac{1}{\Gamma(\xi)\delta^{\xi}} Q\left(\sqrt{2^{\nu}\overline{\gamma}e^{y_1}} - A\right) + O_{W_1}, \end{aligned} \tag{38}$$

where $W_1$ is the number of sample points for approximation, $y_1 = \ln\beta_1$ denotes the integral point, $\zeta_{w_1}$ denotes the weight factors and $O_{W_1}$ is the remainder which is approximate to 0 as $W_1$ approaches infinity.

Substituting $A$ into (38), and integrating (38) with respect to $\beta_{\hat{k}}$, $P_e^{(\mathrm{I})}|_{\mathcal{U}_0}$. can be further calculated as

$$\begin{aligned} P_e^{(\mathrm{I})}|_{\mathcal{U}_0} = &\int_0^{\infty} \left[\sum_{w_1=1}^{W_1} \zeta_{w_1} e^{{y_1}^2} e^{y_1\xi - \frac{e^{y_1}}{\delta}} \frac{1}{\Gamma(\xi)\delta^{\xi}} \right. \\ &\left. Q\left(\sqrt{2^{\nu}\overline{\gamma}e^{y_1}} - \sqrt{2^{\nu}\overline{\gamma}\beta_{\hat{k}}}\mathcal{U}_0\right) + O_{W_1}\right] \frac{{\beta_{\hat{k}}}^{\xi-1}}{\Gamma(\xi)\delta^{\xi}} e^{-\frac{\beta_{\hat{k}}}{\delta}} d\beta_{\hat{k}}. \end{aligned} \tag{39}$$

Let $y_2 = \ln\beta_{\hat{k}}$, and similar to the processing of (38), the closed-form approximation of $P_e^{(\mathrm{I})}|_{\mathcal{U}_0}$. can be given in (40), as shown at the bottom of the next page, where $W_2$ is the number of sample points for approximation, $\zeta_{w_2}$ denotes the weight factors and $O_{W_2}$ is the remainder which is approximate to 0 as $W_2$ approaches infinity. To make the approximation more accurate, $W_1 = W_2 = 80$ is adopted.

Finally, by combining (32), (36), (37) and (40), we can obtain the closed-form expression of $P_b$.

*Proposition 1:* When $\overline{\gamma} \to \infty$, $\frac{1}{2}P_e^{(\mathrm{I})}$ is the error floor for the BEP of the LoRa system over a Rayleigh-lognormal fading channel with *co-SF* interference.

*Proof:* We first deduce the error floor in the case of no interference in (33). When $\overline{\gamma} \to \infty$, since $Q(\sqrt{2^{\nu+1}\overline{\gamma}x} - \sqrt{2H_{2^{\nu}-1}}) = Q(\infty) = 0$, $P_e^{(\mathrm{N})}$ can be approximated to 0. Then, we focus on the error floor in the presence of *co-SF* interference in (37). Similarly, using derivative operation on $P_e^{(\mathrm{I})}$, one can obtain $\frac{\partial P_e^{(\mathrm{I})}}{\partial\overline{\gamma}} = 0$ when $\overline{\gamma} \to \infty$. It implies that $P_e^{(\mathrm{I})}$ is a constant at high SNRs.

$$\begin{aligned} P_e^{(\mathrm{N})} \approx &\frac{a+\frac{1}{2b}}{\Gamma(\xi)}\mathcal{G}\left(\xi, \frac{1}{\delta}\left(a+\frac{1}{2b}\right)\right) + \frac{a-\frac{1}{2b}}{\Gamma(\xi)}\mathcal{G}\left(\xi, \frac{1}{\delta}\left(a-\frac{1}{2b}\right)\right) + \frac{b\delta}{\Gamma(\xi)}\left[\mathcal{G}\left(\xi+1, \frac{1}{\delta}\left(a-\frac{1}{2b}\right)\right) - \mathcal{G}\left(\xi+1, \frac{1}{\delta}\left(a+\frac{1}{2b}\right)\right)\right] \\ \approx &\frac{H_{2^{\nu}-1} - \sqrt{\pi H_{2^{\nu}-1}}}{2^{\nu}\overline{\gamma}\Gamma(\xi)}\mathcal{G}\left(\xi, \frac{1}{\delta}\left(\frac{H_{2^{\nu}-1} - \sqrt{\pi H_{2^{\nu}-1}}}{2^{\nu}\overline{\gamma}}\right)\right) + \frac{H_{2^{\nu}-1} + \sqrt{\pi H_{2^{\nu}-1}}}{2^{\nu}\overline{\gamma}\Gamma(\xi)}\mathcal{G}\left(\xi, \frac{1}{\delta}\left(\frac{H_{2^{\nu}-1} + \sqrt{\pi H_{2^{\nu}-1}}}{2^{\nu}\overline{\gamma}}\right)\right) \\ &- \frac{2^{\nu}\overline{\gamma}\delta}{2\sqrt{\pi H_{2^{\nu}-1}}\Gamma(\xi)}\left[\mathcal{G}\left(\xi+1, \frac{1}{\delta}\left(\frac{H_{2^{\nu}-1} + \sqrt{\pi H_{2^{\nu}-1}}}{2^{\nu}\overline{\gamma}}\right)\right) - \mathcal{G}\left(\xi+1, \frac{1}{\delta}\left(\frac{H_{2^{\nu}-1} - \sqrt{\pi H_{2^{\nu}-1}}}{2^{\nu}\overline{\gamma}}\right)\right)\right]. \end{aligned} \tag{36}$$

$$P_e^{(\mathrm{I})} \approx \frac{\sum_{\tau=0}^{2^{\nu-1}}\left[\frac{1}{2^{\nu}}\sum_{I_1=0}^{2^{\nu}-1}\int_0^{\infty}\int_0^{\infty} Q\left(\sqrt{2^{\nu}\overline{\gamma}\beta_1} - \sqrt{2^{\nu}\overline{\gamma}\beta_{\hat{k}}}\mathcal{U}_0\right) p_{\beta}(\beta_1)p_{\beta}\left(\beta_{\hat{k}}\right)d\beta_1 d\beta_{\hat{k}}\right]}{2^{\nu-1}+1} \approx \frac{\sum_{\tau=0}^{2^{\nu-1}}\left[\frac{1}{2^{\nu}}\sum_{I_1=0}^{2^{\nu}-1} P_e^{I}|_{\mathcal{U}_0}\right]}{2^{\nu-1}+1}. \tag{37}$$

**TABLE 2.** SF specific threshold $q_\nu$ ($B = 125$ KHz).

| Annulus | $\nu$ | SNR $q_\nu$ (dBm) | Range (m) |
|---|---|---|---|
| 1 | 7 | $-6$ | $l_0$–$l_1$ |
| 2 | 8 | $-9$ | $l_1$–$l_2$ |
| 3 | 9 | $-12$ | $l_2$–$l_3$ |
| 4 | 10 | $-15$ | $l_3$–$l_4$ |
| 5 | 11 | $-17.5$ | $l_4$–$l_5$ |
| 6 | 12 | $-20$ | $l_5$–$R$ |

Therefore, we can determine the error floor in the presence of co-SF interference by substituting a high SNR value into (37). ■

*Remark 1:* Based on *Proposition 1*, the error floors of BEP occurs in high SNR region, and the diversity order of the proposed system is zero.

### B. COVERAGE PROBABILITY

In interference-free scenarios, the system is affected by fading and the noise. If the received SNR is below the reception threshold $q_\nu$, which is shown in Table 2, that allows successful detection, the node can not connect to the gateway. By definition, the connection probability is formulated as

$$\mathrm{P_{SNR}} = \mathbb{P}\big[\gamma \geq q_\nu | d_1\big], d_1 \in \big[l_{j-1}, l_j\big]. \tag{41}$$

To find the transmission range when using LoRa signals for WBAN, we need to find the relationship between the distance $d_1$ and the connection probability. By using $\gamma$ in (26), the connection probability can be computed as

$$\begin{aligned}\mathrm{P_{SNR}}(d_1) &= \mathbb{P}\left[\frac{\mathcal{P}_{\mathrm{tx}}}{N}|\hbar_1|^2 g(d_1) \geq q_\nu\right] \\ &= \mathbb{P}\left[|\hbar_1|^2 \geq \frac{N q_\nu}{\mathcal{P}_{\mathrm{tx}} g(d_1)}\right] \\ &= 1 - F_\beta\left(\frac{N q_\nu}{\mathcal{P}_{\mathrm{tx}} g(d_1)}\right) \\ &\approx 1 - \frac{1}{\Gamma(\xi)}\mathcal{G}\left(\xi, \frac{N q_\nu}{\mathcal{P}_{\mathrm{tx}} g(d_1)\delta}\right).\end{aligned} \tag{42}$$

where $\mathbb{P}[\,\cdot\,]$ is the notation for calculating probability.

We can see from (42) that the connection probability is affected by the distance $d_1$ and the transmitted power $\mathcal{P}_{\mathrm{tx}}$. Increasing the transmitted power at the same distance can achieve higher connection probability and thus improving the communication reliability.

Considering an interference scenario, since we use the assumption that different SFs are perfectly orthogonal to one another, the system is able to provide full protection for concurrent transmissions from different SFs. Moreover, except for the case where the smallest SF is used by a very large number of EDs, we only need to consider the dominant *co-SF* interferer. The transmitted power of EDs with the same SF signals are supposed to be equal. Due to the capture effect of the LoRa, the stronger signals will suppress weaker signals received at the same time [28]. We define the strongest interferer $\hat{k}$ as

$$\begin{aligned}\hat{k} &= \arg\max_{k>1}\left\{\mathcal{P}_{\mathrm{tx}}\chi_k^\nu |h_k|^2\right\} \\ &= \arg\max_{k>1}\left\{\mathcal{P}_{\mathrm{tx}}\chi_k^\nu |\hbar_k|^2 g(d_k)\right\},\end{aligned} \tag{43}$$

where $d_k$ and $\hbar_k$ denote the distance and the channel gain between the $k$-th interfering node and the gateway, respectively. Hence, the received SIR of the desired ED under dominant *co-SF* interference is given by

$$\rho = \frac{\mathcal{P}_{\mathrm{tx}}|\hbar_1|^2 g(d_1)}{\hat{\mathcal{I}}}, \tag{44}$$

where $\hat{\mathcal{I}} = \mathcal{P}_{\mathrm{tx}}|\hbar_{\hat{k}}|^2 g(d_{\hat{k}})$ is the dominant *co-SF* interference.

After we find $\hat{k}$, the SIR success probability can be written as

$$\begin{aligned}\mathrm{P_{SIR}}(d_1) &= \mathbb{P}\left[\frac{|\hbar_1|^2 g(d_1)}{|\hbar_{\hat{k}}|^2 g(d_{\hat{k}})} \geq \theta \middle| d_1\right] \\ &= \mathbb{E}_{|\hbar_1|^2}\left[\mathbb{P}\left[X_{\hat{k}} \leq \frac{|\hbar_1|^2 g(d_1)}{\theta}\middle| |\hbar_1|^2, d_1\right]\right],\end{aligned} \tag{45}$$

where $\mathbb{E}[\,\cdot\,]$ represents the statistical expectation, $X_{\hat{k}} = |\hbar_{\hat{k}}|^2 g(d_{\hat{k}})$, and $\theta = 1$ dB is the SIR threshold [27]. If the desired signal is $\theta$ dB stronger than any other signal received simultaneously, no collision occurs.

To find the SIR success probability under the strongest interferer, let $X_i = |\hbar_i|^2 g(d_i)$. According to the previous analysis, since $d_1 \in [l_{j-1}, l_j]$, we can obtain that $|\mathcal{V}_{d_1}| = \pi(l_j^2 - l_{j-1}^2)$ and $\mathcal{V}_{d_1} \subset \mathcal{V}$. Moreover, the PDF of $d_i$, which is defined as the distance between the gateway and the randomly selected ED within the same annulus $\mathcal{V}_{d_1}$, can be written as $f_{d_i}(x) = \frac{2\pi x}{|\mathcal{V}_{d_1}|}$. Hence, the PDF of $g(d_i)$ can be calculated as

$$\begin{aligned}f_{g(d_i)}(x) &= \left|\frac{d}{dx}g^{-1}(x)\right| f_{d_i}\left(g^{-1}(x)\right) \\ &= \frac{2\pi \times 10^{-\frac{2P_L(d_0)}{10n}} x^{-\frac{2}{n}-1}}{n|\mathcal{V}_{d_1}|},\end{aligned} \tag{46}$$

$$P_e^{(\mathrm{I})}\big|_{\mathcal{U}_0} = \frac{1}{\left(\Gamma(\xi)\delta^\xi\right)^2}\sum_{w_2=1}^{W_2}\sum_{w_1=1}^{W_1}\left[\zeta_{w_2} e^{{y_2}^2} e^{y_2\xi - \frac{e^{y_2}}{\delta}}\left(\zeta_{w_1} e^{{y_1}^2} e^{y_1\xi - \frac{e^{y_1}}{\delta}} Q\left(\sqrt{2^\nu \overline{\gamma} e^{y_1}} - \sqrt{2^\nu \overline{\gamma} e^{y_2}}\mathcal{U}_0\right) + O_{W_1}\right)\right] + O_{W_2}. \tag{40}$$

where $g(l_j) \leq x \leq g(l_{j-1})$. Using (30), the approximated closed-form PDF of $X_i$ can be computed as

$$\begin{aligned} f_{X_i}(z) &= f_{g(d_i)}(z) \otimes p_\beta(z) \\ &= \int_{g(l_j)}^{g(l_{j-1})} \frac{1}{x} f_{g(d_i)}(x) p_\beta\left(\frac{z}{x}\right) dx \\ &\approx \int_{g(l_j)}^{g(l_{j-1})} \frac{1}{x} \frac{2\pi \times 10^{-\frac{2P_L(d_0)}{10n}}}{n|\mathcal{V}_{d_1}|} x^{-\frac{2}{n}-1} \frac{1}{\Gamma(\xi)\delta^\xi} \left(\frac{z}{x}\right)^{\xi-1} e^{-\frac{z}{x\delta}} dx \\ &\approx \frac{2\pi \times 10^{-\frac{2P_L(d_0)}{10n}}}{n|\mathcal{V}_{d_1}|\Gamma(\xi)} \left(\frac{1}{\delta}\right)^{-\frac{2}{n}} z^{-\frac{2}{n}-1} \mathcal{G}\left(\frac{2}{n}+\xi, \frac{z}{\delta g(x)}\right)\Big|_{x=l_{j-1}}^{x=l_j}, \end{aligned} \tag{47}$$

where the symbol $\otimes$ stands for convolution and $z > 0$. By integrating (47) and exchanging the order of integration, the CDF of $X_i$ can be given in (48), as shown at the bottom of the page.

According to the order statistics, the CDF of the maximum interference is $F_{X_{\hat{k}}}(z) = \mathbb{E}_{\mathcal{M}}[[F_{X_i}(z)]^{\mathcal{M}}]$, where the sample size $\mathcal{M}$ is a Poisson distributed random variable with mean $\upsilon = \lambda_u |\mathcal{V}_{d_1}|$ and $\upsilon$ is the expected number of concurrently transmitting EDs in the same SF annulus $\mathcal{V}_{d_1}$. Since the value of $\mathcal{M}$ is an integer from 0 to infinity, according to the total probability theorem, one has

$$F_{X_{\hat{k}}}(x) = \sum_{k=0}^{\infty} \frac{\upsilon^k e^{-\upsilon}}{k!} \left[F_{X_i}(x)\right]^k. \tag{49}$$

Using the series formula $e^x = \sum_{k=0}^{\infty} \frac{x^k}{k!}$ and deconditioning on the channel power gain $|\hbar_1|^2$, one can obtain

$$\mathrm{P}_{\mathrm{SIR}}(d_1) = e^{-\upsilon} \int_0^{\infty} e^{\upsilon F_{X_i}\left(\frac{zg(d_1)}{\theta}\right)} p_\beta(z) dz. \tag{50}$$

We can see from (50) that SIR success probability is not only affected by the distance $d_1$, but also the mean of Poisson distributed random variable $\upsilon$, which is related to the channel access mechanisms.

The success probability of the proposed system can be computed as

$$\begin{aligned} \mathrm{P}_{\mathrm{joint}}(d_1) &\approx \mathrm{P}_{\mathrm{SNR}}(d_1)\mathrm{P}_{\mathrm{SIR}}(d_1) \\ &= \left[1 - \frac{1}{\Gamma(\xi)} \mathcal{G}\left(\xi, \frac{Nq_v}{\mathcal{P}_{\mathrm{tx}} g(d_1)\delta}\right)\right] e^{-\upsilon} \\ &\times \int_0^{\infty} e^{\upsilon F_{X_i}\left(\frac{zg(d_1)}{\theta}\right)} p_\beta(z) dz. \end{aligned} \tag{51}$$

Hence, through averaging over $\mathcal{V}$, the coverage probability of the specific ED is given by

$$\mathrm{P_c} = \frac{2}{R^2} \sum_j \int_{l_{j-1}}^{l_j} \mathrm{P}_{\mathrm{joint}}(x) x dx. \tag{52}$$

### C. ENERGY EFFICIENCY

Energy efficiency is defined as the ratio between the number of successfully decoded bits and consumed energy of the system per unit, which represents the efficiency of the system's use of energy resources. In the sleep mode it can be assumed that no ED is working, hence the energy consumption can be negligible. Thus, the energy efficiency for an ED at a distance $x$ from the gateway can be written as

$$\eta_{\mathrm{EE}}(x) = \frac{\mathrm{P}_{\mathrm{joint}}(x) N_{bp}}{E_u}, \tag{53}$$

where $E_u$ is the energy required for transmitting a message to the gateway, which is related to the channel access mechanisms in the network.

According to [28], for the P-ALOHA protocol, one has

$$E_{\text{P-ALOHA}} = \mathcal{P}_{\mathrm{tx}} T_o. \tag{54}$$

For the S-ALOHA protocol, let $\mathcal{P}_{\mathrm{rx}}$ represent the power consumption of an ED when receiving the data, one has

$$E_{\text{S-ALOHA}} = \mathcal{P}_{\mathrm{tx}} T_o + \mathcal{P}_{\mathrm{rx}} T_B \left(\frac{T_o}{\alpha T_{\mathrm{SYN}}}\right), \tag{55}$$

where the synchronization is maintained by the gateway sending periodic beacons of $T_B$ duration every interval $T_{\mathrm{SYN}}$.

For the NP-CSMA, one has

$$E_{\text{NP-CSMA}} = \mathcal{P}_{\mathrm{tx}} T_o + \mathcal{P}_{\mathrm{rx}} T_{\mathrm{CAD}} \left[\frac{\overline{E(n_A)}}{1 - e^{-\overline{E(n_A)}}}\right], \tag{56}$$

where $T_{\mathrm{CAD}}$ is the channel activity detection (CAD) duration, and $\overline{E(n_A)} = \lambda p \pi (l_j^2 - l_{j-1}^2) \Xi$ is the expected number of active neighbors.

Through averaging over $\mathcal{V}$, the average energy efficiency of the proposed system can be computed as

$$\overline{\eta}_{EE} = \frac{2}{R^2} \sum_j \int_{l_{j-1}}^{l_j} \eta_{\mathrm{EE}}(x) x dx. \tag{57}$$

### D. THROUGHPUT

According to Section II, one has a Poisson distributed EDs with the offered traffic $G$, where $G = \alpha\overline{\mathcal{N}}$. The throughput of the proposed system for the $j$-th annulus for all MAC protocols is given by

$$\mathcal{CT}_j = \frac{2G}{R^2} \int_{l_{j-1}}^{l_j} \mathrm{P}_{\mathrm{joint}}(x) x dx. \tag{58}$$

Hence, the average throughput for the area $\mathcal{V}$ is calculated as

$$\overline{\mathcal{CT}} = \sum_j \mathcal{CT}_j. \tag{59}$$

$$F_{X_i}(z) = \int_0^z f_{X_i}(x) dx = \frac{\pi 10^{-\frac{2P_L(d_0)}{10n}}}{|\mathcal{V}_{d_1}|\Gamma(\xi)} \left[g(x)^{-\frac{2}{n}} \mathcal{G}\left(\xi, \frac{z}{\delta g(x)}\right) - \left(\frac{z}{\delta}\right)^{-\frac{2}{n}} \mathcal{G}\left(\frac{2}{n}+\xi, \frac{z}{\delta g(x)}\right)\right]\Big|_{x=l_{j-1}}^{x=l_j}. \tag{48}$$

**TABLE 3.** Some parameters for LoRa.

| Parameters | Symbol | Value |
|---|---|---|
| Bandwidth | $B$ | 125 KHz |
| Carrier Frequency | $f_c$ | 868 MHz |
| Transmit Power | $\mathcal{P}_{\text{tx}}$ | 14 dBm |
| Power Consumption for Received Data | $\mathcal{P}_{\text{rx}}$ | 15.18 mW |
| Pathloss Exponent | $n$ | 2.8 |
| Pathloss | $P_L(d_0)$ | 49.6 dB |
| Message Preamble | $N_{sp}$ | 8 symbols |
| Activity Factor | $\alpha$ | 0.33% |
| Coding Rate | $CR$ | 4/8 |
| Payload | $N_{bp}$ | 10 bytes |
| Guard Interval | $T_g$ | 10.24 ms |
| Detection Threshold | $\mathcal{P}_0$ | -150 dB |
| Beacon Preamble + Payload Synchronization Interval | $T_{\text{SYN}}$ | 128 s |
| CAD Duration | $T_{\text{CAD}}$ | 2 symbols |

### E. DELAY

The delay is defined as the number of transmissions required to successfully transmit a packet. In this paper, we do not consider the processing delay and propagation delay. The delay of the proposed system for the $j$-th annulus for all MAC protocols is given by

$$D_j = \frac{1}{\frac{2}{R^2}\int_{l_{j-1}}^{l_j} \mathrm{P}_{\text{joint}}(x)x dx}. \tag{60}$$

Hence, the average delay for the area $\mathcal{V}$ is calculated as

$$\overline{D} = \sum_j D_j. \tag{61}$$

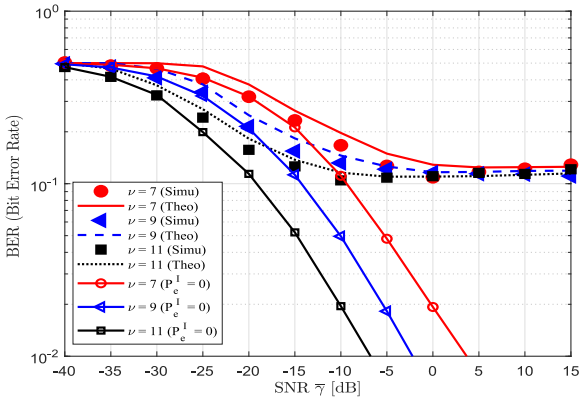


**FIGURE 3.** The theoretical and simulated BEP curves of the proposed system over Rayleigh-lognormal fading channel with no interference and *co-SF* interference for $\nu$ = 7,9,11, where $\sigma_{dB}$ = 8 dB and $\rho$ = 6 dB.

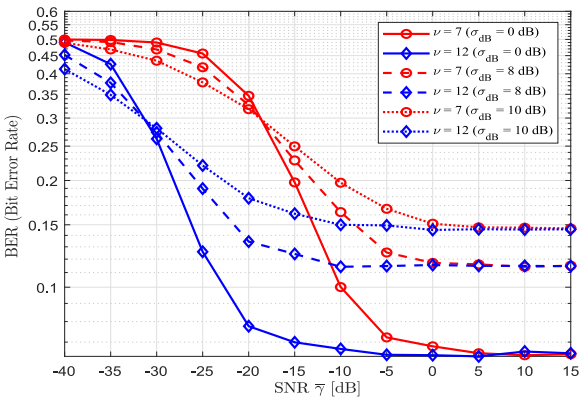


**FIGURE 4.** The simulated BEP curves of the proposed system with various values of $\sigma_{dB}$ and $\nu$ over Rayleigh-lognormal fading channel with *co-SF* interference, where $\rho$ = 6 dB.

## IV. RESULTS AND DISCUSSION

In this section, the analytical results for the proposed network are verified through Monte-Carlo simulations conducted using MATLAB. Some typical parameters are shown in Table 4. The BEP at various SNR levels is computed based on an average of $10^5$ simulation runs. We evaluate the success probability at different distances by averaging results from $10^5$ simulation runs, considering the EDs detected by the activity factor $\alpha$ within area $\mathcal{V}$. Subsequently, the coverage probability is evaluated by averaging the success probability over $\mathcal{V}$. Similarly, energy efficiency, average throughput, and average delay are estimated. Unless otherwise specified, the SFs are allocated based on EIB or EAB scheme, progressing from 7 to 12.

### A. BEP

Fig. 3 presents the theoretical and simulated BEP curves over Rayleigh-lognormal fading channel with no interference and *co-SF* interference for $\nu$ = 7, 9, and 11, respectively, where the standard deviation $\sigma_{dB}$ is 8 dB and the SIR $\rho$ is 6 dB. From this figure, under *co-SF* interference, there is a small gap between the theoretical closed-form results and the simulated results due to the use of approximations in the derivation. The curves with $P_e^{(\text{I})} = 0$ represent the case with no interference. Moreover, it can be observed from this figure that considering the *co-SF* interference, the BEP performance of the LoRa system deteriorates seriously. With increasing the value of $\nu$, better performance can be obtained when $\overline{\gamma} < 5$ dB, while the BEP can be regarded as a fixed value when $\overline{\gamma} \geq 5$ dB. In addition, at the same BEP, the SNR gaps between $\nu = 7$ and $\nu = 9$, $\nu = 9$ and $\nu = 11$ are about 5 dB.

Fig. 4 shows the simulated BEP curves of the proposed system with various values of $\sigma_{dB}$ and $\nu$ over Rayleigh-lognormal fading channel with *co-SF* interference. From this figure, at the same value of $\nu$, better performance can be achieved when decreasing the standard deviation. For example, at a BEP of 0.2 and $\nu = 7$, the SNR gap is about 2.5 dB between $\sigma_{dB} = 10$ dB and $\sigma_{dB} = 8$ dB, and between $\sigma_{dB} = 8$ dB and $\sigma_{dB} = 0$ dB. Secondly, it can be seen that compared to the unshadowed Rayleigh fading channel, the BEP the proposed system over shadowed Rayleigh fading

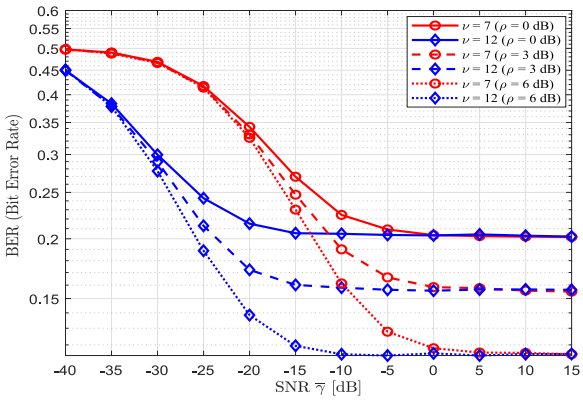


**FIGURE 5.** The simulated BEP curves of the proposed system with various values of $\rho$ and $\nu$ over Rayleigh-lognormal fading channel with *co-SF* interference, where $\sigma_{dB} = 8$ dB.

channel is obviously affected by the shadowing. When $\overline{\gamma} \geq 5$ dB, the BEP gap between unshadowed ($\sigma_{dB} = 0$ dB) and shadowed ($\sigma_{dB} = 8$ dB) Rayleigh fading channel is about 0.12. Furthermore, regardless of the value of $\sigma_{dB}$, if the value of $\sigma_{dB}$ remains the same, the gain for increasing the value of $\nu$ from 7 to 12 are almost constant and is about 12.5 dB when $\overline{\gamma} < 5$ dB.

Fig. 5 shows the simulated BEP curves of the proposed system with various values of $\rho$ and $\nu$ over Rayleigh-lognormal fading channel with *co-SF* interference. From this figure, at the same value of $\nu$, the BEP can be effectively improved by increasing the SIR. For example, when $\overline{\gamma} \geq 5$ dB, the BEP gap is 0.04 between $\rho = 0$ dB and $\rho = 3$ dB, and it is 0.15 between $\rho = 3$ dB and $\rho = 6$ dB.

Based on the above discussions, it can be found that BEP performance of the LoRa system can be improved through increasing the values of $\nu$ and $\rho$, and reducing the value of $\sigma_{dB}$. To reduce the BEP in practical applications, we can increase the SF and the SIR in the environments with low shadow effect, e.g., hilly/moderate-to-heavy tree density ($\sigma_{dB} = 2.3$ dB), hilly light tree density or flat/moderate-to-heavy tree density ($\sigma_{dB} = 3.0$ dB) and flat/light tree density ($\sigma_{dB} = 1.6$ dB) [42]. However, in the mountain ($\sigma_{dB} = 11.9$ dB) and canyon ($\sigma_{dB} = 10.13$ dB) [18], etc., reducing the shadow effect by adjusting the position of the antenna and increasing the SIR by controlling the power are also effective methods to obtain significant performance gain.

### B. COVERAGE PROBABILITY

Fig. 6 shows the coverage probability of the proposed system with respect to average number of EDs for the network radius $R = 1$ km and 6 km. Simulation results verify the theoretical derivations in (42), (50) and (51). It can be observed from Fig. 6 that the coverage probability decreases with the increase of $\overline{\mathcal{N}}$ due to the increase of interfering sources. As shown in Fig. 6 (a), for a small value of $R$, the NP-CSMA protocol can access more number of EDs than the

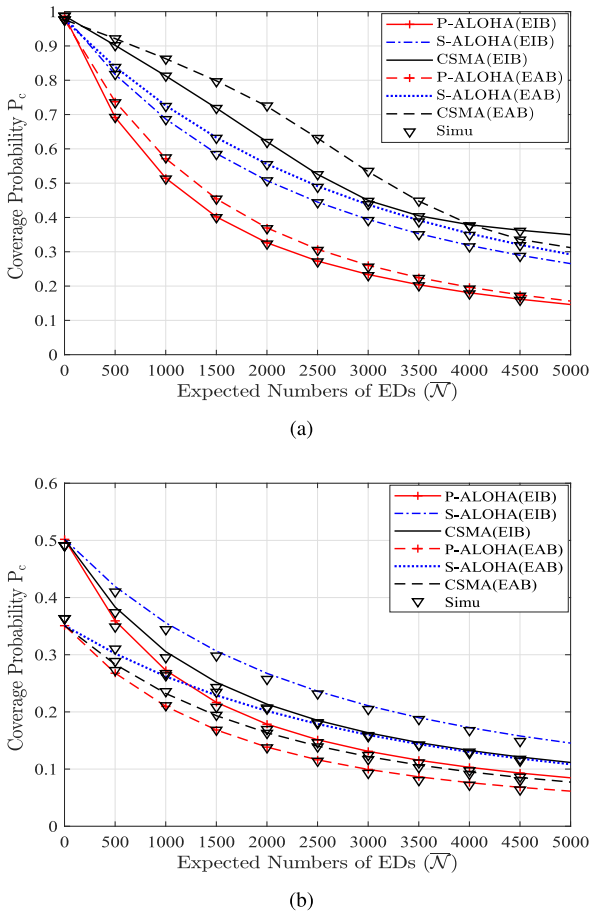


**FIGURE 6.** Coverage probability with respect to average number of EDs for different channel access protocols. (a) $R = 1$ km. (b) $R = 6$ km.

P-ALOHA and S-ALOHA protocol. In addition, the number of EDs that can be accessed by using the EAB scheme is greater than that of the EIB scheme for the three protocols. However, as shown in Fig. 6 (b), for a large value of $R$, more EDs can be accessed via the EIB scheme for each protocol and the S-ALOHA protocol can access more number of EDs. Therefore, the network radius $R$ is an important factor for the choice of SF allocation schemes and the three MAC protocols.

Fig. 7 shows the coverage probability with respect to $R$ for the three MAC protocols, where $\overline{\mathcal{N}} = 3000$, and $\overline{\mathcal{N}} = 5000$. It can seen from these figures that the coverage probability decreases with the increase of the network radius $R$. Moreover, it can be observed that for small value of the network radius $R$, the EAB scheme has a higher coverage probability than the EIB one and the NP-CSMA protocol has a higher coverage probability than the P-ALOHA and S-ALOHA protocols. Furthermore, with the increase of the network radius $R$, the coverage probability of the EAB scheme decreases more than that of the EIB scheme, and the coverage probability of the NP-CSMA protocol decreases more than that of the S-ALOHA protocols. After a specific

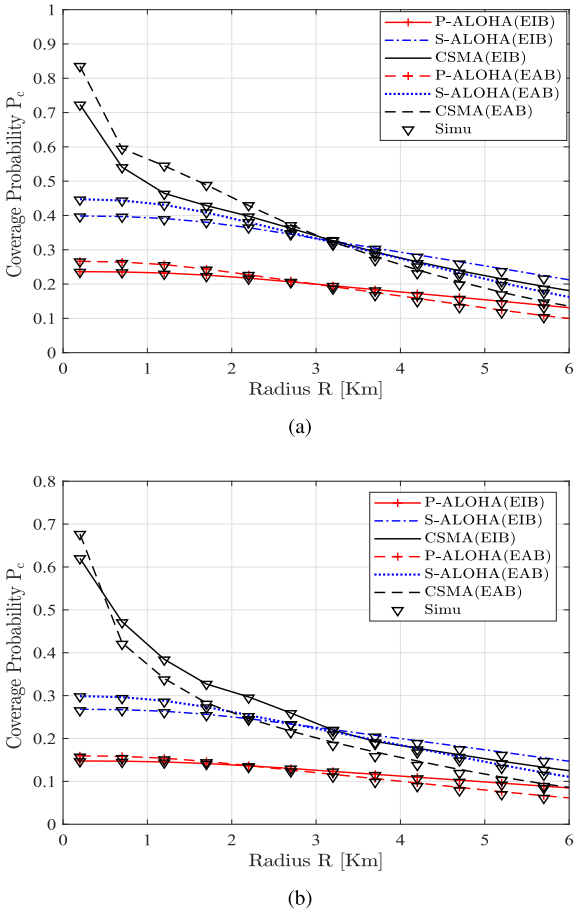


**FIGURE 7.** Coverage probability with respect to network radius $R$ for different channel access protocols. (a) $\overline{\mathcal{N}} = 3000$. (b) $\overline{\mathcal{N}} = 5000$.

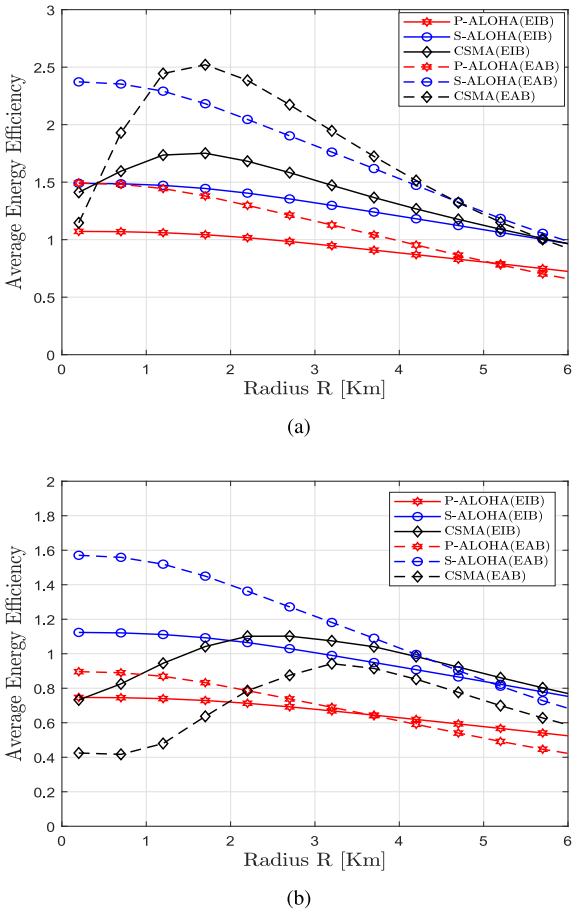


**FIGURE 8.** Average energy efficiency with respect to network radius $R$ for different channel access protocols. (a) $\overline{\mathcal{N}} = 3000$. (b) $\overline{\mathcal{N}} = 5000$.

value of the network radius $R$, the coverage probability of the EIB scheme exceeds the EAB scheme, the coverage probability of the S-ALOHA protocols exceeds the NP-CSMA protocol. With increasing the number of EDs, the coverage probability of the EIB scheme exceeds that of the EAB scheme at a smaller value of the network radius $R$. Consequently, to obtain higher coverage probability, for a small value of $R$, the EAB scheme performs better than the EIB scheme, and the NP-CSMA protocol is more efficient than the P-ALOHA and S-ALOHA protocols. As shown in Fig. 7 (b), the EAB scheme can yield an improvement of up to 353% when compared to the EIB scheme (see the NP-CSMA versus P-ALOHA curves for an $R = 0.2$ km). For a large value of $R$, the EIB scheme and the S-ALOHA protocol could be adopted. The EIB scheme can yield an improvement of up to 180% when compared to the EAB scheme (see the S-ALOHA versus P-ALOHA curves for an $R = 6$ km).

### C. ENERGY EFFICIENCY

Fig. 8 shows the average energy efficiency curves of the proposed system with different values of $R$, where $\overline{\mathcal{N}} = 3000$ and 5000. It can be found that when the number of EDs is fixed, there exists the value of $R$ to reach the optimal average energy efficiency for the NP-CSMA protocol. For example, when $\overline{\mathcal{N}} = 3000$, the NP-CSMA protocol has an optimal value of the average energy efficiency, i.e., $R \approx 1.8$ km shown in Fig. 8 (a). From Fig. 8 (a) and (b), it can be seen that for the P-ALOHA and S-ALOHA protocol, the EAB scheme performs better than the EIB scheme for a small value of $R$ regardless of the value of $\overline{\mathcal{N}}$. For the NP-CSMA protocol, the EAB scheme performs better than the EIB scheme in a certain range of $R$ when $\overline{\mathcal{N}} = 3000$, while for $\overline{\mathcal{N}} = 5000$, better result can be achieved by using the EIB scheme regardless of the value of $R$. As shown in Fig. 8 (b), the EAB scheme can yield an improvement of up to 273% (see the S-ALOHA versus NP-CSMA curves for an $R = 0.2$ km). As shown in Fig. 8 (a), The EIB scheme can yield an improvement of up to 49% when compared to the EAB scheme (see the S-ALOHA versus P-ALOHA curves for an $R = 6$ km). While the EIB scheme can yield an improvement of up to 83% when compared to the EAB scheme (see the NP-CSMA versus P-ALOHA curves for an $R = 6$ km), as shown in Fig. 8 (b). Therefore, from the

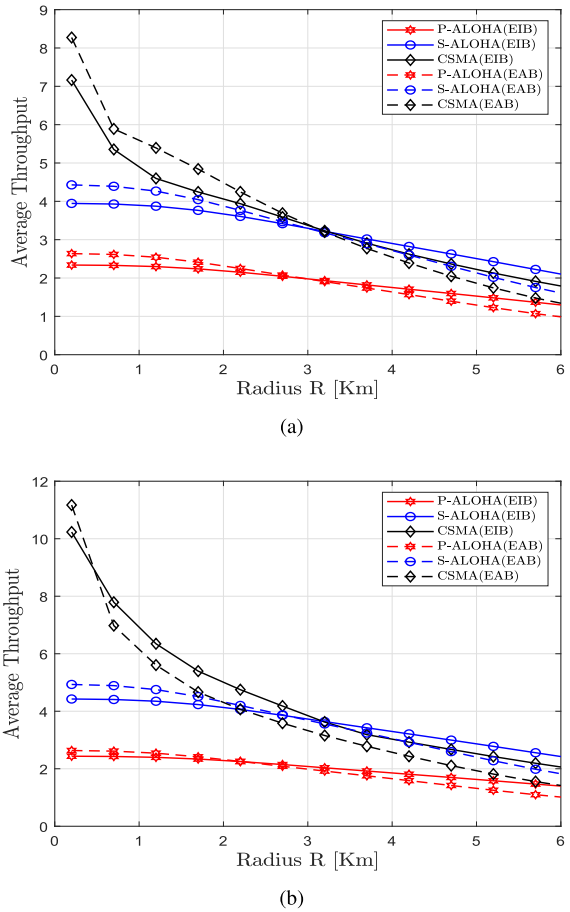


**FIGURE 9.** Average throughput with respect to network radius $R$ for different channel access protocols. (a) $\overline{\mathcal{N}} = 3000$. (b) $\overline{\mathcal{N}} = 5000$.

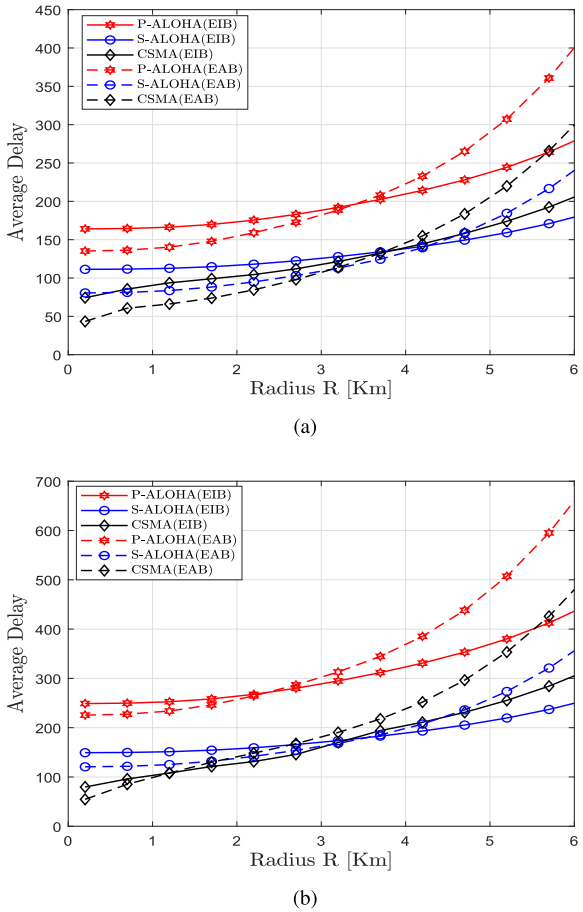


**FIGURE 10.** Average delay with respect to network radius $R$ for different channel access protocols. (a) $\overline{\mathcal{N}} = 3000$. (b) $\overline{\mathcal{N}} = 5000$.

perspective of energy efficiency, in practical applications, the EAB scheme with the S-ALOHA protocol is suitable for a small value of $R$, while for a large value of $R$, with the increase of $\overline{\mathcal{N}}$, the EIB scheme with the NP-CSMA protocol can be utilized.

### D. THROUGHPUT

Fig. 9 shows the average throughput of the three MAC protocols for different values of $R$, where $\overline{\mathcal{N}} = 3000$ and 5000. It can be seen that to obtain higher throughput, the EAB scheme with the NP-CSMA protocol can be adopted for small network radius, while the EIB scheme with the S-ALOHA protocol can be used for large network radius. The conclusion is the same as that of the coverage probability from Fig. 7. As shown in Fig. 9 (b), the EAB scheme can yield an improvement of up to 360% when compared to the EIB scheme (see the NP-CSMA versus P-ALOHA curves for an $R = 0.2$ km). The EIB scheme can yield an improvement of up to 144% when compared to the EAB scheme (see the S-ALOHA versus P-ALOHA curves for an $R = 6$ km).

### E. DELAY

Fig. 10 shows the average delay of the three MAC protocols for different values of $R$, where $\overline{\mathcal{N}} = 3000$ and 5000. From Fig. 10, it can be found that the increase of the network radius leads to an increase in the delay for a fixed number of EDs. By comparing Fig. 10 (a) with Fig. 10 (b), increasing the number of EDs with a fixed network radius also leads to an increase in delay. From the perspective of delay, the EIB scheme with the S-ALOHA can be used for large network radius, otherwise the EAB scheme with NP-CSMA protocol can be adopted. As shown in Fig. 9 (b), the EAB scheme can yield an improvement of up to 78% when compared to the EIB scheme (see the NP-CSMA versus P-ALOHA curves for an $R = 0.2$ km). The EIB scheme can yield an improvement of up to 63% when compared to the EAB scheme (see the S-ALOHA versus P-ALOHA curves for an $R = 6$ km).

*Remark 2:* Based on the above analyses, we can choose the appropriate SF allocation schemes and MAC protocols to design the system under different performance metrics (i.e., coverage probability, energy efficiency, throughput and delay), and different usage environments (i.e., large or small network radius, a large or small number of EDs). We summarize the insights for future LoRa-based WBAN designs in Table 4.

**TABLE 4.** Design for future LoRa-based WBAN.

| Usage environments / Performance metrics | Small network radius | Large network radius | |
|---|---|---|---|
| | | A small number of EDs | A large number of EDs |
| High coverage probability | EAB scheme + S-ALOHA protocol | EIB scheme + NP-CSMA protocol | |
| High average throughput | | | |
| Low average delay | | | |
| High energy efficiency | | EIB scheme + S-ALOHA protocol | EIB scheme + NP-CSMA protocol |

## V. CONCLUSION

In this paper, the performance of the LoRa system for WBAN has been investigated from PHY and MAC layers over Rayleigh-lognormal fading channel with *co-SF* interference. The closed-form BEP expression of the LoRa system under Rayleigh-lognormal fading channel and *co-SF* interference has been derived. The results show that increasing the value of SF $\nu$ and SIR $\rho$, and decreasing the value of standard deviation $\sigma_{dB}$ are effective ways to resist the shadowed effect in different environments. Moreover, the performance of the P-ALOHA, S-ALOHA and NP-CSMA protocols for the LoRa based WBAN has been analyzed in terms of coverage probability, energy efficiency, throughput and system delay. Furthermore, the performance of the EIB and EAB schemes for the LoRa based WBAN has also been investigated. From the theoretical and simulated results, it can be found that to obtain higher coverage probability and throughput, and lower delay, the EIB scheme with the S-ALOHA protocol can be adopted for large network radius, and can obtain a maximum improvement of 180%, 144%, and 63%, respectively. In addition, the EAB scheme with the NP-CSMA protocol is suggested for small network radius, and can obtain a maximum improvement of 353%, 360%, and 78%, respectively. To achieve higher energy efficiency, the EAB scheme with the S-ALOHA protocol can be chosen for small network radius, and can obtain a maximum improvement of 273%. For large network radius, the EIB scheme with the S-ALOHA protocol and the EIB scheme with the NP-CSMA protocol are suitable for a small number of EDs and a large number of EDs, respectively, and can obtain a maximum improvement of 49% and 83%, respectively. Thanks to the these advantages, LoRa communication can be considered as a promising candidate for the WBAN.

## REFERENCES


[1] Y. A. Qadri, A. Nauman, Y. B. Zikria, A. V. Vasilakos, and S. W. Kim, "The future of healthcare Internet of Things: A survey of emerging technologies," *IEEE Commun. Surveys Tuts.*, vol. 22, no. 2, pp. 1121–1167, 2nd Quart., 2020.

[2] S. D. Robinsha and B. Amutha, "IoT revolutionizing healthcare: A survey of smart healthcare system architectures," in *Proc. Int. Conf. Res. Methodol. Knowl. Manag., Artif. Intell. Telecommun. Eng. (RMKMATE)*, 2023, pp. 1–5.

[3] H. Habibzadeh, K. Dinesh, O. R. Shishvan, A. Boggio-Dandry, G. Sharma, and T. Soyata, "A survey of healthcare Internet of Things (HIoT): A clinical perspective," *IEEE Internet Things J.*, vol. 7, no. 1, pp. 53–71, Jan. 2020.

[4] "IEEE standard for local and metropolitan area networks part 15.6: Wireless body area networks," IEEE Standard 802.15.6-2012, 2012.

[5] A. Elik, K. N. Salama, and A. M. Eltawil, "The Internet of bodies: A systematic survey on propagation characterization and channel modeling," *IEEE Internet Things J.*, vol. 9, no. 1, pp. 321–345, Jan. 2022.

[6] J. Wang and Q. Wang, *Body Area Communications: Channel Modeling, Communication Systems, and EMC*. Hoboken, NJ, USA: Wiley, 2012.

[7] L. Liu, J. Shi, F. Han, X. Tang, and J. Wang, "In-body to on-body channel characterization and modeling based on heterogeneous human models at HBC-UWB band," *IEEE Sensors J.*, vol. 22, no. 20, pp. 19772–19785, Oct. 2022.

[8] M. I. Waly et al., "Advancement of a high-efficiency wearable antenna enabling wireless body area networks," *IEEE Access*, vol. 11, pp. 138325–138335, 2023.

[9] P. K. Bishoyi and S. Misra, "Priority-aware cooperative data uploading in body-to-body networks for healthcare IoT," *IEEE Internet Things J.*, vol. 9, no. 12, pp. 10319–10326, Jun. 2022.

[10] A. Mondal, M. Hanif, and H. H. Nguyen, "SSK-ICS LoRa: A LoRa-based modulation scheme with constant envelope and enhanced data rate," *IEEE Commun. Lett.*, vol. 26, no. 5, pp. 1185–1189, May 2022.

[11] C. Milarokostas, D. Tsolkas, N. Passas, and L. Merakos, "A comprehensive study on LPWANs with a focus on the potential of LoRa/LoRaWAN systems," *IEEE Commun. Surveys Tuts.*, vol. 25, no. 1, pp. 825–867, 1st Quart., 2023.

[12] P. Gkotsiopoulos, D. Zorbas, and C. Douligeris, "Performance determinants in LoRa networks: A literature review," *IEEE Commun. Surveys Tuts.*, vol. 23, no. 3, pp. 1721–1758, 3rd Quart., 2021.

[13] M. S. Islam, M. T. Islam, A. F. Almutairi, G. K. Beng, N. Misran, and N. Amin, "Monitoring of the human body signal through the Internet of Things (IoT) based LoRa wireless network system," *Appl. Sci.*, vol. 9, no. 9, p. 1884, May 2019.

[14] H. Zhang, G. Liu, Y. Xu, and T. Jiang, "LoRaAid: Underground joint communication and localization system based on LoRa technology," *IEEE Trans. Wireless Commun.*, early access, Oct. 24, 2023, doi: 10.1109/TWC.2023.3325330.

[15] H. Taleb, A. Nasser, G. Andrieux, N. Charara, and E. M. Cruz, "Energy consumption improvement of a healthcare monitoring system: Application to LoRaWAN," *IEEE Sensors J.*, vol. 22, no. 7, pp. 7288–7299, Apr. 2022.

[16] S. Benaissa et al., "Joint antenna-channel modelling for in-to-out-body propagation of dairy cows at 868 MHz," in *Proc. 14th Eur. Conf. Antennas Propag. (EuCAP)*, 2020, pp. 1–4

[17] T. Ameloot, P. Van Torre, and H. Rogier, "LoRa base-station-to-body communication with SIMO front-to-back diversity," *IEEE Trans. Antennas Propag.*, vol. 69, no. 1, pp. 397–405, Jan. 2021.

[18] G. M. Bianco, R. Giuliano, G. Marrocco, F. Mazzenga, and A. Mejia-Aguilar, "LoRa system for search and rescue: Path-loss models and procedures in mountain scenarios," *IEEE Internet Things J.*, vol. 8, no. 3, pp. 1985–1999, Feb. 2021.

[19] T. Elshabrawy and J. Robert, "Closed-form approximation of LoRa modulation BER performance," *IEEE Commun. Lett.*, vol. 22, no. 9, pp. 1778–1781, Sep. 2018.

[20] O. Georgiou and U. Raza, "Low power wide area network analysis: Can LoRa scale?" *IEEE Wireless Commun. Lett.*, vol. 6, no. 2, pp. 162–165, Apr. 2017.

[21] A. Valach and D. Macko, "Upper confidence bound based communication parameters selection to improve scalability of LoRa @FIIT communication," *IEEE Sensors J.*, vol. 22, no. 12, pp. 12415–12427, Jun. 2022.

[22] M. Jouhari, N. Saeed, M.-S. Alouini, and E. M. Amhoud, "A survey on scalable LoRaWAN for massive IoT: Recent advances, potentials, and challenges," *IEEE Commun. Surveys Tuts.*, vol. 25, no. 3, pp. 1841–1876, 3rd Quart., 2023.
[23] S. Lee, J. Lee, H.-S. Park, and J. K. Choi, "A novel fair and scalable relay control scheme for Internet of Things in LoRa-based low-power wide-area networks," *IEEE Internet Things J.*, vol. 8, no. 7, pp. 5985–6001, Apr. 2021.
[24] T. Polonelli, D. Brunelli, A. Marzocchi, and L. Benini, "Slotted ALOHA on LoRaWAN–Design, analysis, and deployment," *Sensors*, vol. 19, no. 4, p. 838, Feb. 2019.
[25] T.-H. To and A. Duda, "Simulation of LoRa in NS-3: Improving LoRa performance with CSMA," in *Proc. IEEE Int. Conf. Commun. (ICC)*, 2018, pp. 1–7.
[26] C. Pham, "Robust CSMA for long-range LoRa transmissions with image sensing devices," in *Proc. Wireless Days (WD)*, 2018, pp. 116–122.
[27] A. Mahmood, E. Sisinni, L. Guntupalli, R. Rondón, S. A. Hassan, and M. Gidlund, "Scalability analysis of a LoRa network under imperfect orthogonality," *IEEE Trans. Ind. Informat.*, vol. 15, no. 3, pp. 1425–1436, Mar. 2019.
[28] L. Beltramelli, A. Mahmood, P. Österberg, and M. Gidlund, "LoRa beyond ALOHA: An investigation of alternative random access protocols," *IEEE Trans. Ind. Informat.*, vol. 17, no. 5, pp. 3544–3554, May 2021.
[29] M. Haenggi and R. K. Ganti, "Interference in large wireless networks," Norwell, MA, USA: Now Publ., 2009.
[30] C. K. Armeniakos and A. G. Kanatas, "Performance comparison of wireless aerial 3D cellular network models," *IEEE Commun. Lett.*, vol. 26, no. 8, pp. 1779–1783, Aug. 2022.
[31] S. Srinivasa and M. Haenggi, "Distance distributions in finite uniformly random networks: Theory and applications," *IEEE Trans. Veh. Technol.*, vol. 59, no. 2, pp. 940–949, Feb. 2010.
[32] J. Shi, Y. Takagi, D. Anzai, and J. Wang, "Performance evaluation and link budget analysis on dual-mode communication system in body area networks," *IEICE Trans. Commun.*, vol. 97, no. 6, pp. 1175–1183, 2014.
[33] O. Afisiadis, S. Li, J. Tapparel, A. Burg, and A. Balatsoukas-Stimming, "On the advantage of coherent LoRa detection in the presence of interference," *IEEE Internet Things J.*, vol. 8, no. 14, pp. 11581–11593, Jul. 2021.
[34] T. Elshabrawy and J. Robert, "Analysis of BER and coverage performance of LoRa modulation under same spreading factor interference," in *Proc. IEEE 29th Annu. Int. Symp. Pers., Indoor Mobile Radio Commun. (PIMRC)*, 2018, pp. 1–6.
[35] A. M. Mathai, "*An Introduction to Geometrical Probability Distributional Aspects with Applications*. Portland, OR, USA: Scitech Book News, 1999.
[36] A. Abdi and M. Kaveh, "On the utility of gamma pdf in modeling shadow fading (slow fading)," in *Proc. IEEE 49th Veh. Technol. Conf.*, 1999, pp. 2308–2312
[37] A. Furtado, J. Pacheco, and R. Oliveira, "PHY/MAC uplink performance of LoRa class a networks," *IEEE Internet Things J.*, vol. 7, no. 7, pp. 6528–6538, Jul. 2020.
[38] S. Al-Ahmadi and H. Yanikomeroglu, "On the approximation of the generalized-K distribution by a gamma distribution for modeling composite fading channels," *IEEE Trans. Wireless Commun.*, vol. 9, no. 2, pp. 706–713, Feb. 2010.
[39] B. Makki and M.-S. Alouini, "End-to-end performance analysis of delay-sensitive multi-relay networks," *IEEE Commun. Lett.*, vol. 23, no. 12, pp. 2159–2163, Dec. 2019.
[40] O. Afisiadis, M. Cotting, A. Burg, and A. Balatsoukas-Stimming, "On the error rate of the LoRa modulation with interference," *IEEE Trans. Wireless Commun.*, vol. 19, no. 2, pp. 1292–1304, Feb. 2020.
[41] M. Abramowitz and I. A. Stegun, "Handbook of mathematical functions: With formulas, graphs, and mathematical tables," in *Handbook of Mathematical Functions: With Formulas*. Mineola, NY, USA: Dover Publ., 1970.
[42] B. T. Sieskul, F. Zheng, and T. Kaiser, "On the effect of shadow fading on wireless geolocation in mixed LOS/NLOS environments," *IEEE Trans. Signal Process.*, vol. 57, no. 11, pp. 4196–4208, Nov. 2009.

**MINLING ZHANG** received the B.Sc. degree in electronic and information engineering from the Dongguan University of Technology, Dongguan, China, in 2021. She is currently pursuing the M.Sc. degree in information and communication engineering with the Guangdong University of Technology, Guangzhou, China. Her primary research interests include wireless body area networks, LoRa networks, and Internet of Things.

**GUOFA CAI** (Senior Member, IEEE) received the B.S. degree in communication engineering from Jimei University, Xiamen, China, in 2007, the M.S. degree in circuits and systems from Fuzhou University, Fuzhou, China, in 2012, and the Ph.D. degree in communication engineering from Xiamen University, Xiamen, China, in 2015. In 2017, he was a Research Fellow with the School of Electrical and Electronic Engineering, Nanyang Technological University, Singapore. He is currently an Associate Professor with the School of Information Engineering, Guangdong University of Technology, China. His primary research interests include information theory and coding, spread-spectrum modulation, wireless body area networks, and Internet of Things.

**ZHIPING XU** (Member, IEEE) received the Ph.D. degree in information and communication engineering from Xiamen University, Xiamen, China, in 2021. He is currently a Lecturer with the School of Ocean Information Engineering, Jimei University, Xiamen. His current research interests include channel coding/decoding, joint source-channel coding/decoding, coded modulation and their applications to wireless communication, underwater acoustic communications, maritime communication, semantic communication, wireless body area networks, and the Internet of Things.

**JIGUANG HE** (Senior Member, IEEE) received the Ph.D. degree in communications engineering from the University of Oulu, Finland, in 2018. He serves currently as a Senior Researcher with the Technology Innovation Institute, Abu Dhabi, UAE, and holds a Docentship (also known as an Adjunct Professor) with the University of Oulu. From September 2013 to March 2015, he was affiliated with the State Key Laboratory of Terahertz and Millimeter Waves, City University of Hong Kong, focusing on beam tracking within millimeter-wave MIMO systems. Subsequently, from June 2015 to August 2021, he was associated with the Centre for Wireless Communications, University of Oulu, initially as a Doctoral Researcher and later as a Postdoctoral Researcher. He served as an Assistant Professor with the Macau University of Science and Technology from August 2021 to March 2022. He has actively contributed to numerous international and national projects, including EU FP7 RESCUE, EU H2020 ARIADNE, and the 6G Flagship, and received one FDCT-GDST Joint Research Project from Macau Science and Technology Development Fund. His research interests span integrated sensing and communications, reconfigurable intelligent surfaces, millimeter-wave MIMO communications, and advanced signal processing techniques. He received the Best Paper Award from IEEE ICCT 2023. He is recognized as an Exemplary Reviewer of IEEE TRANSACTIONS ON COMMUNICATIONS and IEEE COMMUNICATIONS LETTERS, and he serves as a technical program committee member for various IEEE conferences. He currently serves as an Associate Editor for IEEE TRANSACTIONS ON VEHICULAR TECHNOLOGY.

**MARKKU JUNTTI** (Fellow, IEEE) received the M.Sc. and D.Sc. degrees in EE from the University of Oulu, Oulu, Finland, in 1993 and 1997, respectively.

From 1992 to 1998, he was with the University of Oulu. From 1994 to 1995, he was a Visiting Scholar with Rice University, Houston, TX, USA. From 1999 to 2000, he was a Senior Specialist with Nokia Networks, Oulu, Finland. He has been a Professor of Communications Engineering with the Centre for Wireless Communications (CWC), University of Oulu since 2000. He serves as the Leader of CWC – Radio Technologies Research Unit. He is also an Adjunct Professor with the Department of Electrical and Computer Engineering, Rice University, Houston, TX, USA. He is an author or a coauthor in almost 500 papers published in international journals and conference records as well as in books *Wideband CDMA for UMTS* from 2000 to 2010, *Handbook of Signal Processing Systems* in 2013 and 2018, and *5G Wireless Technologies* in 2017. His research interests include signal processing for wireless networks as well as communication and information theory.

Dr. Juntti is an Editor of IEEE TRANSACTIONS ON WIRELESS COMMUNICATIONS, and served previously in similar role in IEEE TRANSACTIONS ON COMMUNICATIONS and IEEE TRANSACTIONS ON VEHICULAR TECHNOLOGY. He was a Secretary of IEEE Communication Society Finland Chapter from 1996 to 1997 and the Chair from 2000 to 2001. He has been a Secretary of the Technical Program Committee of the 2001 IEEE International Conference on Communications, and the Chair or the Co-Chair of the Technical Program Committee of several conferences, including 2006 and 2021 IEEE International Symposium on Personal, Indoor and Mobile Radio Communications, the Signal Processing for Communications Symposium of IEEE Globecom 2014, Symposium on Transceivers and Signal Processing for 5G Wireless and mm-Wave Systems of IEEE GlobalSIP 2016, ACM NanoCom 2018, 2019 International Symposium on Wireless Communication Systems, and 2024 IEEE International Symposium on Joint Communications and Sensing. He has also served or serves as the General Chair of 2011 IEEE Communication Theory Workshop in 2011, 2022 IEEE Workshop on Signal Processing Advances in Wireless Communications, and 2025 IEEE Joint Communications and Sensing Symposium.